Vibrational Spectroscopy of Thin Organic Films

Vasilis G. Gregoriou[1] and Sheila E. Rodman[2]

[1] *Institute of Chemical Engineering and High Temperature Processes – Foundation of Research & Technology–Hellas (ICE/HT-FORTH), Patras, Greece*
[2] *Polaroid Corporation, Waltham, MA, USA*

1 INTRODUCTION

In this article an overview of the applications of vibrational spectroscopic techniques to thin organic films will be presented and selective publications that deal with the application of IR and Raman spectroscopies to thin organic films, Langmuir–Blodgett (LB) films and self-assembled monolayers (SAMs) will be shown. Generally, the amount of the sample is very low when we are dealing with ultrathin organic films so specific experiments need to be performed to extract the vibrational signatures of these molecules. Commonly used techniques in the infrared region are the difference infrared reflection-absorption spectroscopy (IRRAS) and its polarization modulation (PM) analog based on the use of a photoelastic modulator, known as polarization modulation infrared reflection-absorption spectroscopy (PM-IRRAS). The reader should consult the articles by Umemura, **Reflection–Absorption Spectroscopy of Thin Films on Metallic Substrates**, and Weibel and Frey, **Polarization-modulation Approaches to Reflection–Absorption Spectroscopy**, on the theory and instrumentation of IRRAS and PM-IRRAS, respectively, for a better understanding of the experimental considerations on how to perform these types of experiments.

Under the general name of thin organic films, we include any polymeric layer(s) and coatings that range in thickness from angstroms to a few microns. Two categories of ultrathin samples that have their own importance are SAMs and LB films, and they will be discussed separately.

© John Wiley & Sons Ltd, 2002.

For general discussions on thin organic film preparation and characterization, the reader may consult several recent texts and reviews by Ulman[1–3] and Dluhy.[4]

2 APPLICATIONS TO SAMS

SAMs have been used extensively to produce ultrathin and ordered films in two dimensions. Infrared reflection spectroscopy has been used extensively for their characterization, since it provides both molecular recognition as well as information about the spatial configuration of the molecules that constitute the SAMs.

In a recent study, the reversible protection and reactive patterning of amine- and hydroxyl-terminated SAMs on gold surfaces for the fabrication of biopolymer arrays has been investigated using PM-IRRAS among other techniques.[5] In this study, the base-labile protecting group 9-fluorenyl-methoxy-carbonyl (Fmoc) and the acid-labile protecting group dimethoxytrityl (DMT) were used to protect the alkanethiol SAMs. The reactivity and wettability of different portions of the surface can thus be controlled by this reversible protection chemistry. The reaction of the amine-terminated alkanethiol 11-mercaptoundecylamine (MUAM) on a gold surface with an *N*-hydroxysuccinimide (NHS) ester derivative of Fmoc formed a covalent urethane (carbamate) linkage and converted the initially hydrophilic MUAM surface to a hydrophobic, Fmoc-terminated surface. Figure 1 shows the Fmoc protection reactions in detail.

The Fmoc was cleaved upon exposure of the Fmoc-modified surface to a solution of a secondary amine, regenerating the original hydrophilic MUAM surface. Fmoc can also be utilized as a hydroxyl protecting group, as

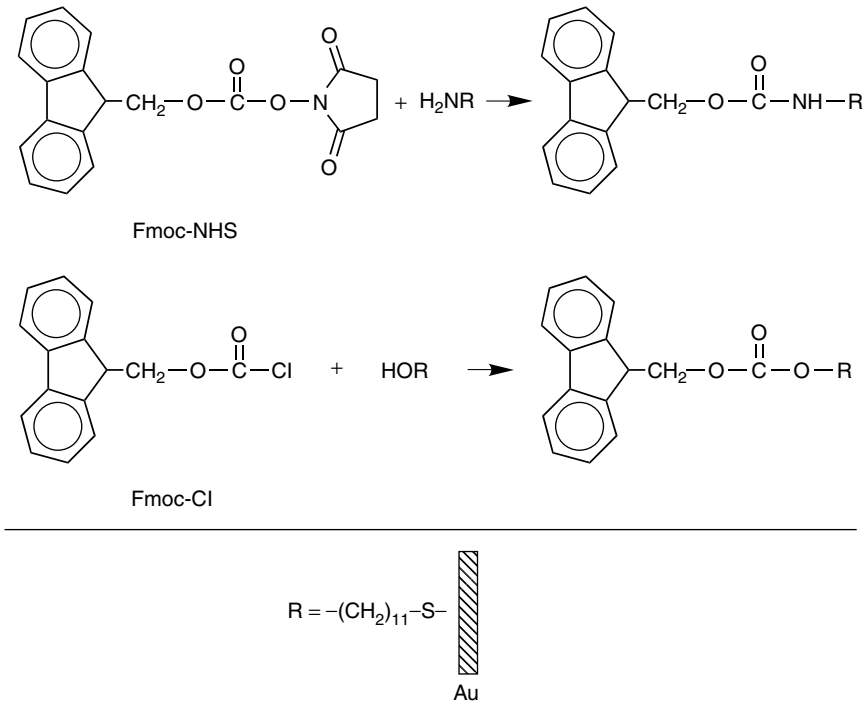

Figure 1. Fmoc protection reactions of the amine- and hydroxyl-terminated alkanethiol SAMs. [Reproduced by permission of the American Chemical Society from A.G. Frutos, J.M. Brockman and R.M. Corn, *Langmuir*, **16**, 2192 (2000).]

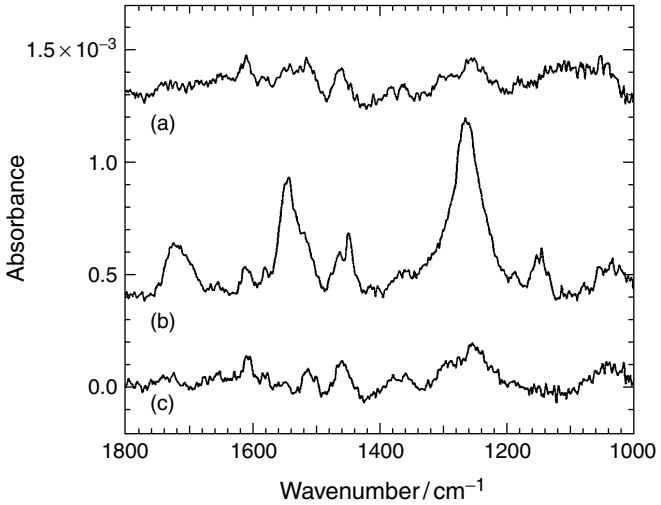

Figure 2. PM-IRRAS spectra of the protection and deprotection of the MUAM SAM. (a) Initial MUAM monolayer. (b) After reaction with Fmoc. (c) After removal of Fmoc. [Reproduced by permission of the American Chemical Society from A.G. Frutos, J.M. Brockman and R.M. Corn, *Langmuir*, **16**, 2192 (2000).]

demonstrated by the reaction of Fmoc-Cl with a monolayer of 11-mercaptoundecanol (MUD). The hydrophobic protecting group DMT was reacted with the ω-hydroxyl groups of both MUD and poly(ethylene glycol)-terminated alkanethiol SAMs to form an acid labile ether bond. The DMT group was removed by soaking the surface in 3% trifluoracetic acid. Figure 2 displays the PM-IRRAS spectra of the protection and deprotection of the MUAM SAM. The presence of the bands at $1720\,cm^{-1}$ ($\nu_{C=O}$), $1544\,cm^{-1}$ (CHN vibration) and $1267\,cm^{-1}$ (coupled CN and C=O stretch) in the spectrum of MUAM-Fmoc indicates the formation of the carbamate linkage. The similarity of the spectra of the original MUAM to the deprotected MUAM is proof of the complete removal of the Fmoc.

In another series of papers that dealt with novel optically responsive materials, the orientation characteristics of sulfonated polystyrene/poly(diallyldimethylammonium chloride) (SPS/PDAC) ionic polymer multilayers on patterned SAMs was investigated.[6,7] This polymeric thin film of alternating bilayers was fabricated by ionic multilayer assembly. The molecular template consisted of patterned SAMs of ω-functionalized alkane thiolates. Alternating layers of polyanion and polycation were then selectively adsorbed onto specific regions of the surface to form patterned films of thickness from 150 to 400 Å. Figure 3 shows a representation of the SAM with the polymer multilayers.

It was found that the polyion conformation played a crucial role in the selectivity of the patterned film, film surface characteristics, and ultimately the ability of these systems to function as optical devices. Figure 4 shows the normalized PM-IRRAS spectra of a 13 bilayer system in the presence and absence of 1 M NaCl.

The IR spectroscopic data revealed that the molecular orientation of polyions in these structures depends on the ionic content of the initial solutions. The addition of salt

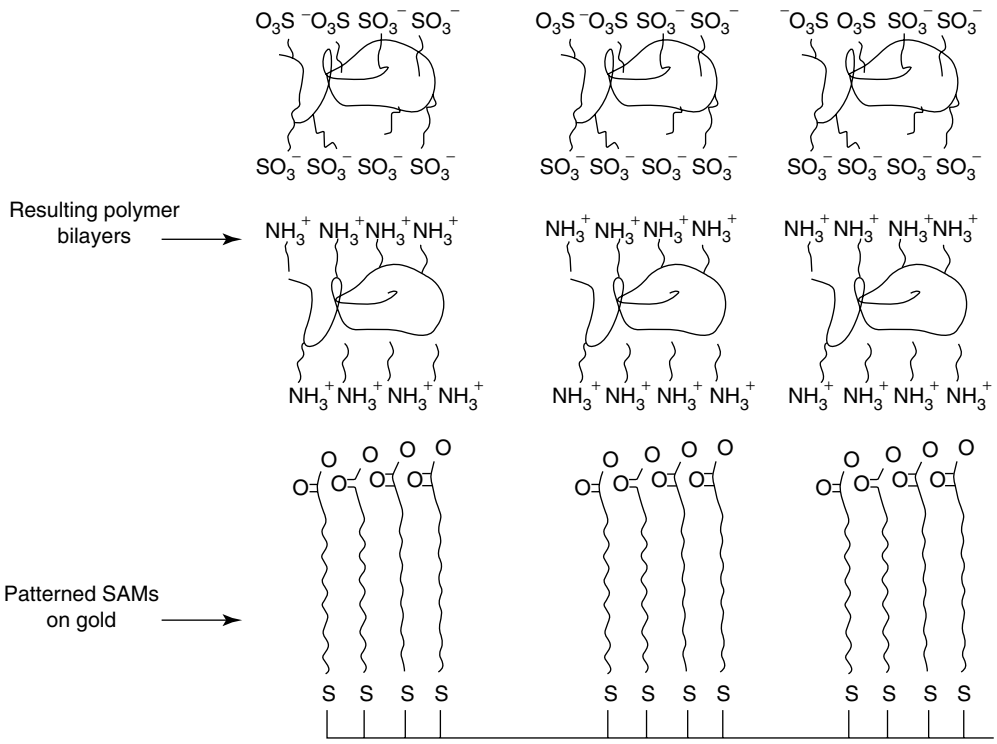

Figure 3. Representation of the patterned SAM with polymer multilayers. [Reproduced by permission of the Society for Applied Spectroscopy from V.G. Gregoriou, R. Hapanowicz, S.L. Clark and P.T. Hammond, *Appl. Spectrosc.*, **51**, 470 (1997).]

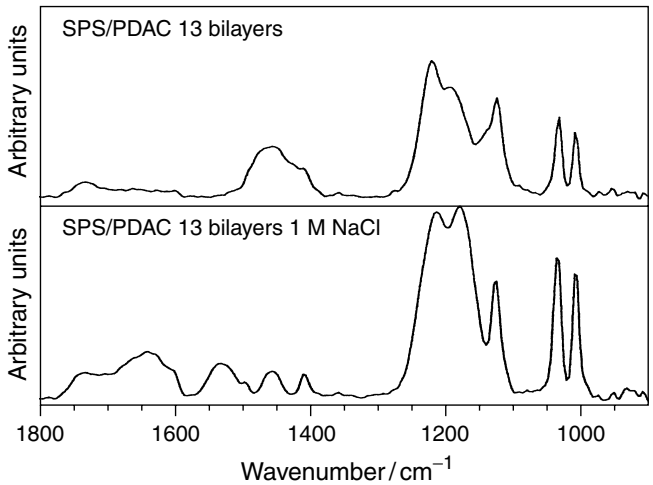

Figure 4. Normalized PM-IRRAS spectra of a 13-bilayer system in the presence and absence of 1 M NaCl. [Reproduced by permission of the Society for Applied Spectroscopy from V.G. Gregoriou, R. Hapanowicz, S.L. Clark and P.T. Hammond, *Appl. Spectrosc.*, **51**, 470 (1997).]

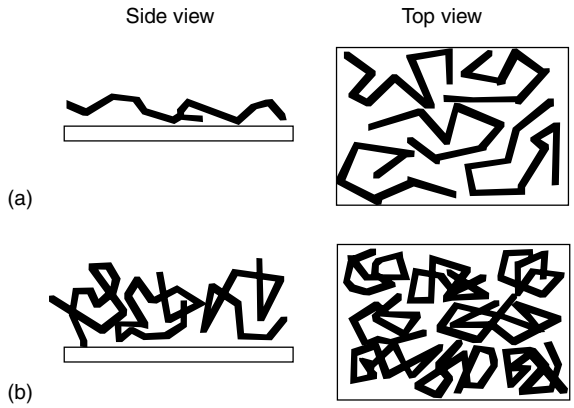

Figure 5. Arrangement of the polymeric chains: (a) no electrolyte present; (b) 1 M NaCl present. [Reproduced by permission of the Society for Applied Spectroscopy from V.G. Gregoriou, R. Hapanowicz, S.L. Clark and P.T. Hammond, *Appl. Spectrosc.*, **51**, 470 (1997).]

shielded the charge along the polymer backbone, allowing polymer chain segments to interact. Figure 5 depicts the proposed arrangement of the polymeric chains based on the PM-IRRAS data.

In addition, the spectroscopic characterization of noncentrosymmetric azobenzene/zirconium phosphonate (ZP) multilayer films that show very interesting electro-optical properties included PM-IRRAS studies.[8] Figure 6 presents a schematic diagram for the construction of noncentrosymmetric ZP multilayer films that incorporate the asymmetric azobenzene chromophore [5-[4-[4-[[(6-hydroxyhexyl)sulfonyl]phenyl]azo]phenyl]pentoxy]phosphonic acid (HAPA).

Figure 7 shows the mid-infrared region of the PM-IRRAS spectrum of a seven-layer ZP/HAPA film on a

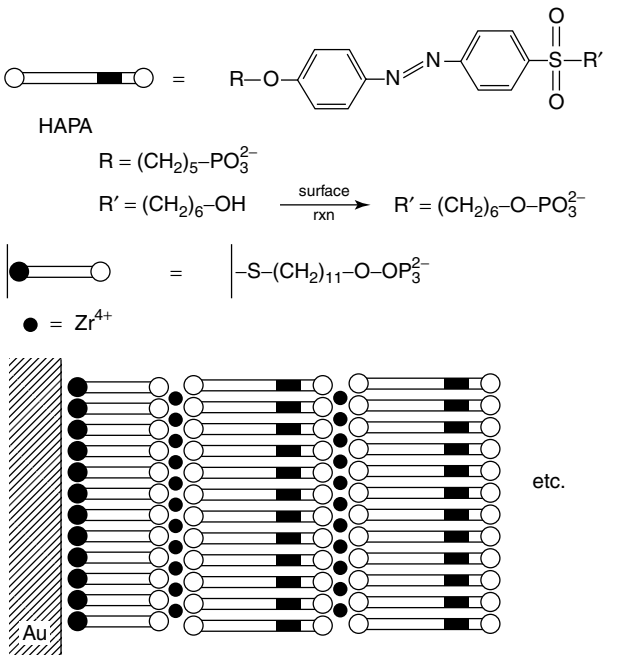

Figure 6. Schematic diagram for the construction of noncentrosymmetric ZP multilayer films on gold. [Reproduced by permission of the American Chemical Society from D.G. Hanken, R.R. Naujok, J.M. Gray and R.M. Corn, *Anal. Chem.*, **69**, 240 (1997).]

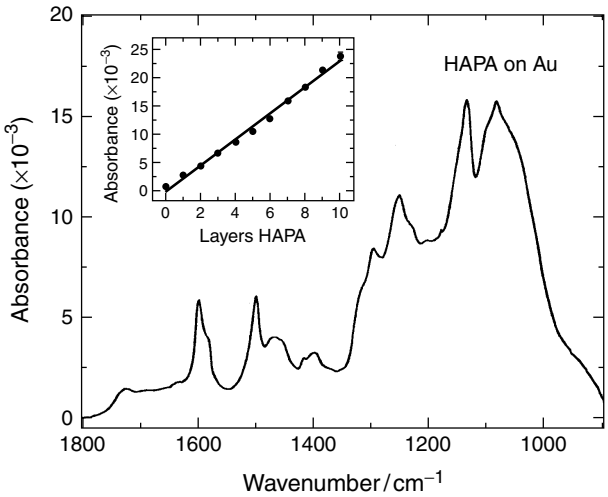

Figure 7. PM-IRRAS spectrum of a seven-layer ZP/HAPA film on a vapor-deposited thin gold film. Inset graph: intensity of the $1140\,cm^{-1}$ symmetric sulfonyl stretching band as a function of the number of HAPA monolayers. [Reproduced by permission of the American Chemical Society from D.G. Hanken, R.R. Naujok, J.M. Gray and R.M. Corn, *Anal. Chem.*, **69**, 240 (1997).]

vapor-deposited thin gold film. It is evident from the inset graph that there is a linear dependence between the intensity of the $1140\,cm^{-1}$ band and the number of HAPA monolayers.

In addition to PM-IRRAS, these films were characterized by surface plasmon resonance (SPR) and optical second

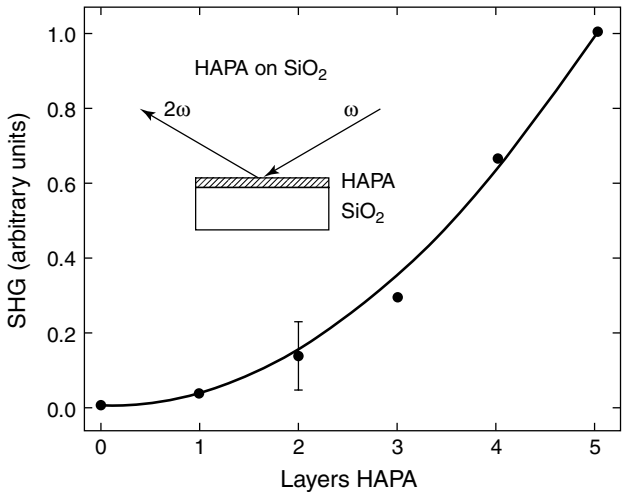

Figure 8. Observed SHG intensity for a five-layer ZP/HAPA film. [Reproduced by permission of the American Chemical Society from D.G. Hanken, R.R. Naujok, J.M. Gray and R.M. Corn, *Anal. Chem.*, **69**, 240 (1997).]

harmonic generation (SHG). The average monolayer thickness of the HAPA multilayer films was found to be 27 ± 0.5 Å by SPR measurement. The resonant SHG at 365 nm from ultrathin ZP/HAPA films on silica surfaces increased quadratically with the number of self-assembled HAPA monolayers. Figure 8 presents the observed SHG intensity for a five-layer ZP/HAPA film.

The focus of another recent study was the kinetics, functionalization and photopatterning of SAMs on polymer surfaces.[9] In this study, monolayers of bifunctional bolaamphiphiles (amphiphiles containing two identical head groups) were self-assembled on a polymeric substrate. This substrate was a spin-coated film of poly(allylamine hydrochloride) (PAAm). The bolaamphiphiles used are symmetrically substituted bis(benzoic acid azide) 4,4′-[(1,12-dioxo-1,12-dodecanediyl)diimino]bisbenzoyl azide (DBAzC10). Various features of the novel bifunctional, well-ordered, and relatively stiff monolayer and the subsequent reactions of the exposed benzoyl azide groups were examined. IRRAS and ellipsometry were used for the characterization of the monolayers and to follow the kinetics of self-assembly. Figure 9 shows the kinetics of self-assembly, as a series of IRRAS spectra illustrating the evolution of the surface monolayer indicated by the increase in azide peaks.

Molecular modeling and ellipsometry studies found that the bolaamphiphiles in the monolayers were inclined at an angle of about 68° to the normal and that the monomolecular layers appeared to be fairly crystalline. A stable, dense, well-ordered, two-dimensional monomolecular layer of bolaamphiphiles was achieved by serial functionalization of the exposed benzoyl azide groups. The initial reaction with dansylcadaverine (DCV) in the liquid phase converted approximately 50% of the benzoyl azide

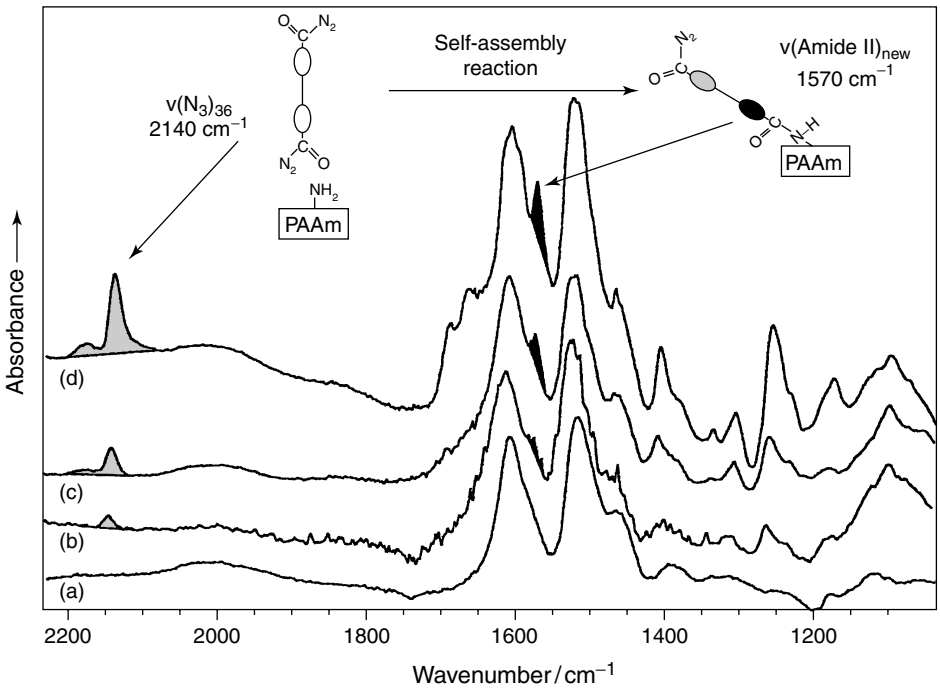

Figure 9. Kinetics of self-assembly of DBAzC10 molecules on PAAm. (a) Spin-coated PAAm film on gold-coated slide; (b) after 90 min; (c) after 180 min; (d) after 600 min. [Reproduced by permission of the American Chemical Society from P. Boehme, G. Vedantham, T. Przybycien and G. Belfort, *Langmuir*, **15**, 5323 (1999).]

groups. The second step, reaction with propylamine in the gas phase, rapidly converted the remaining azide groups. Figure 10 depicts the kinetics of the surface reaction of self-assembled DBAzC10.

Photopatterning, via UV irradiation of exposed benzoyl azide groups, was also demonstrated. Figure 11 shows the photopatterning of the DBAzC10 SAM. The disappearance of the 2140 cm^{-1} azide stretching band demonstrated the effectiveness of the UV irradiation.

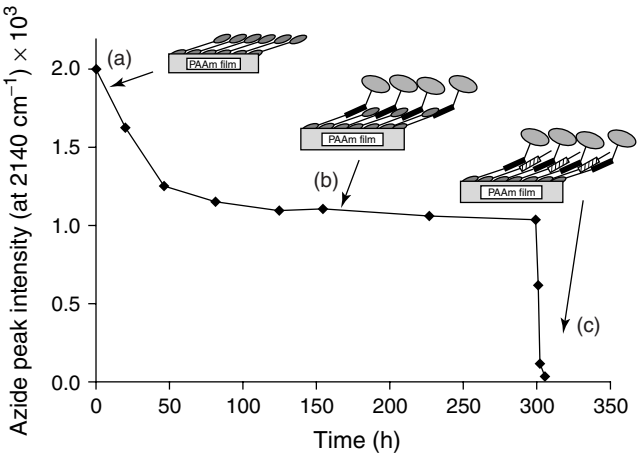

Figure 10. Kinetics of the surface reaction of self-assembled DBAzC10 with DCV followed by reaction with propylamine gas. (a) Initial azide. (b) Decay due to reaction with DCV. (c) Fast reaction of remaining azide groups with propylamine. [Reproduced by permission of the American Chemical Society from P. Boehme, G. Vedantham, T. Przybycien and G. Belfort, *Langmuir*, **15**, 5323 (1999).]

In a study where long-range electron transfer was considered, photocurrent was produced by photoexcitation of a SAM in the presence of an electron donor or acceptor.[10] Specifically, SAMs of a series of α-helical tridecapeptides or heneicosapeptides containing an *N*-ethylcarbazolyl (ECz) at one end and a disulfide group at the other were prepared on gold. ECz-A12-SS and ECz-A20-SS have the ECz group on the N terminal whereas SS-A12-ECz has the disulfide on the N terminal. The ECz group functions as a photosensitizer. The helix tilt angles from the surface normal were found to be about 40° by IRRAS. In the presence of the electron acceptor methyl viologen (MV^{2+}), electron donation from a gold surface to an ECz group was observed upon photoexcitation. Figures 12 and 13 show the IRRAS spectrum of the ECz-A12-SS SAM and the schematic diagram of the cathodic photocurrent generation in the presence of MV^{2+}, respectively.

The direction of photocurrent was reversed in the presence of electron donors such as triethanolamine (TEOA) or ethylenediaminetetraacetic acid (EDTA). In the case of the anodic photocurrent generation using TEOA, the largest photocurrent was observed for SS-A12-ECz SAM. This implies that the electron donation from an ECz group to a gold surface was accelerated by the helix dipole moment directing toward the gold surface. The electronic coupling between an ECz group and a gold surface through the

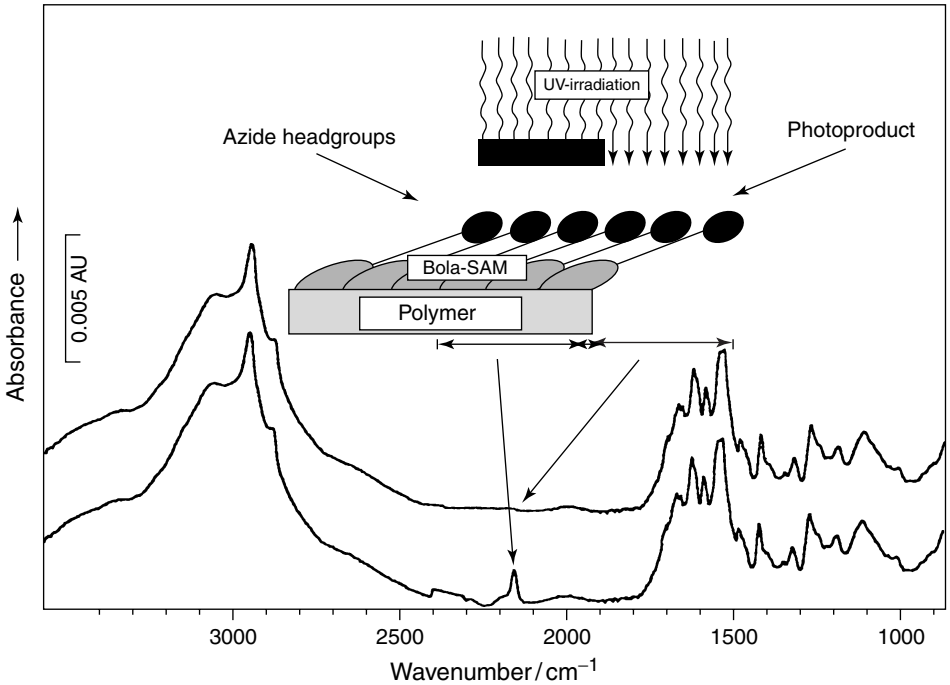

Figure 11. Photopatterning of the DBAzC10 SAM. IRRAS spectra before and after UV irradiation at 300 nm for 120 s. Note disappearance of azide band at 2140 cm^{-1}. [Reproduced by permission of the American Chemical Society from P. Boehme, G. Vedantham, T. Przybycien and G. Belfort, *Langmuir*, **15**, 5323 (1999).]

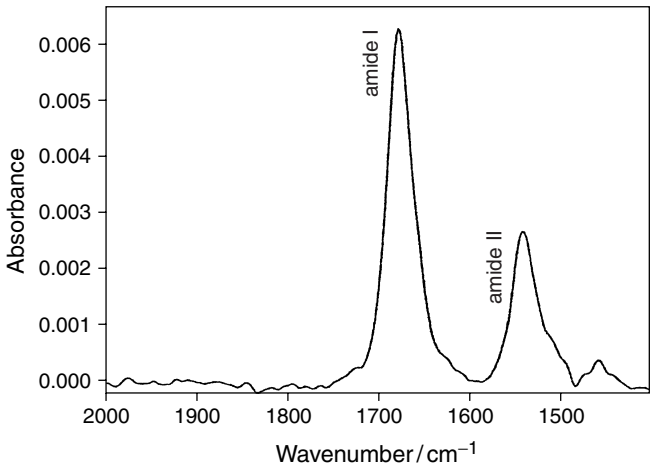

Figure 12. IRRAS spectrum of the ECz-A12-SS SAM. [Reproduced by permission of the American Chemical Society from T. Morita, S. Kimura, S. Kobayashi and Y. Imanishi, *J. Am. Chem. Soc.*, **122**, 2850 (2000).]

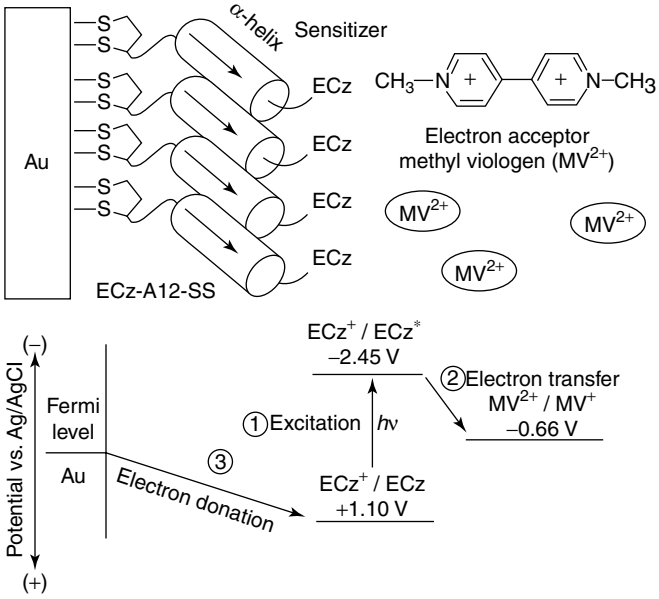

Figure 13. Schematic diagram of the cathodic photocurrent generation in the presence of MV^{2+}. [Reproduced by permission of the American Chemical Society from T. Morita, S. Kimura, S. Kobayashi and Y. Imanishi, *J. Am. Chem. Soc.*, **122**, 2850 (2000).]

peptide molecule was found to occur more strongly than through the saturated hydrocarbon ECz-C11-SS. The helical peptides were therefore shown as an excellent medium for electron transfer. Figure 14 provides the measured photocurrents of the various SAMs upon irradiation with monochromatic light of 351 nm.

The attachment of cadmium sulfide (CdS) nanoparticles to SAMs of alkanethiols on gold was another system that benefited from the use of IRRAS data.[11] Mono- and multilayers of CdS nanoparticles were fabricated on a gold substrate covered with either 1,6-hexanedithiol or 1,10-decanedithiol SAMs by sequential immersion of the substrate into the ethanolic dithiol solution and

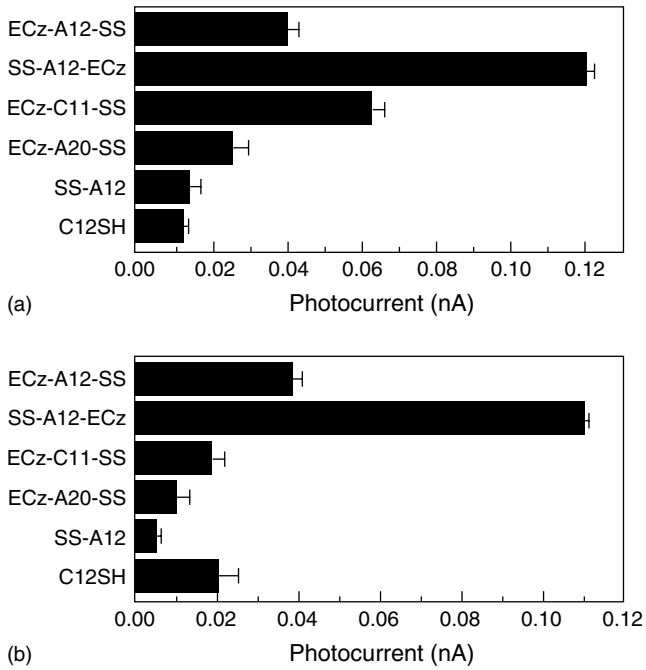

Figure 14. Measured anodic photocurrents of the SAMs in aqueous TEOA (a) and in EDTA solution (b). [Reproduced by permission of the American Chemical Society from T. Morita, S. Kimura, S. Kobayashi and Y. Imanishi, *J. Am. Chem. Soc.*, **122**, 2850 (2000).]

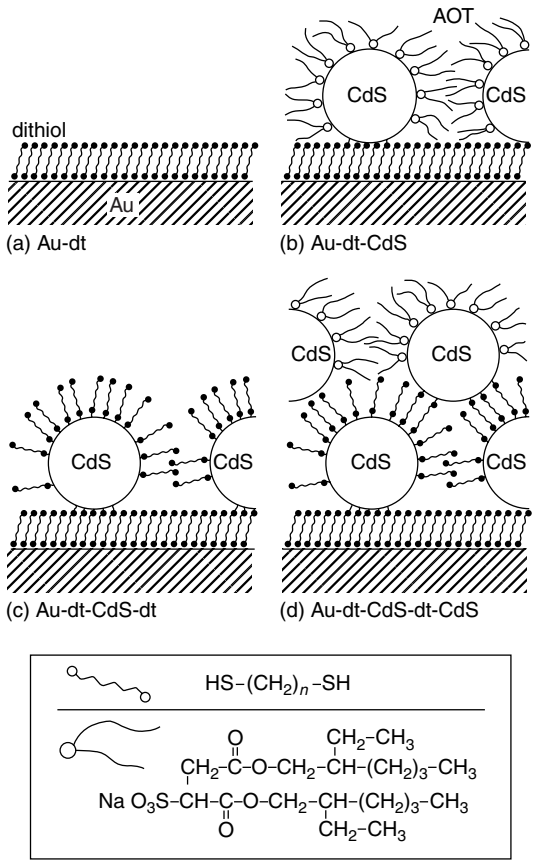

Figure 15. Schematic of the binding of CdS nanoparticles from reversed micelles. (a) Dithiol SAM on Au. (b) CdS nanoparticles attached onto SAM. (c) Adsorption of dithiol onto the CdS nanoparticles. (d) Formation of second CdS nanoparticle layer. [Reproduced by permission of the American Chemical Society from T. Nakanishi, B. Ohtani and K. Uosaki, *J. Phys. Chem. B*, **102**, 1571 (1998).]

a dispersion of 3 nm diameter CdS nanoparticles. The CdS dispersion was prepared in sodium bis(2-ethylhexyl)-sulfosuccinate (Aerosol OT, AOT)/H_2O/heptane reversed micelles. Figure 15 depicts a schematic illustration of the binding of the CdS nanoparticles from reversed micelles.

IRRAS data among others revealed that the CdS nanoparticles on SAMs were surrounded by AOT, which was then substituted by dithiols when the film was treated with the dithiol solution. Figure 16 shows the CH stretching region of the hexanedithiol and decanedithiol SAM, along with the transmission spectrum of the decanethiol for comparison. The photoinduced anodic current was observed when the composite film was immersed in an electrolyte solution containing TEOA as an electron donor.

Also, the sequential deposition of self-assembled ZP molecular monolayers containing two different bisphosphonate ions, 1,10-decanediylbis(phosphonate) (DBP) and 4,4′-azodibenzenediylbis(phosphonate) (AZO) was used to fabricate ultrathin (submicrometer) organic films of specified index of refraction.[12] The ratio of DBP to AZO monolayers in the ZP multilayer film controlled the index of refraction. A combination of SPR measurements and PM-IRRAS was used to examine the structure of the ZP multilayers on vapor-deposited gold substrates. The average thickness of the SAMs was greater in the mixed films than in either the 100% DBP or 100% AZO multilayers. Ellipsometric measurements determined the index of refraction of the ZP multilayers on transparent substrates. ZP films consisting of 100% DBP and 100% AZO molecules were found to have indexes of refraction of 1.51 and 1.64, respectively, at an optical wavelength of 632.8 nm. The data indicated that the index of refraction of the mixed ZP multilayers could be varied systematically between 1.51 and 1.64.

Finally, the relationship between the redox behavior and structure/orientation changes of the SAM of 4-$EtOC_6H_4N$:NC_6H_4CONH $(CH_2)_{10}SH$-4 on a gold electrode surface was studied by electrochemical in-situ IRRAS.[13] Figure 17 shows the schematic drawing of the azo SAM on the gold surface.

The bands observed in the potential dependent IRRAS spectra corresponded well to the reduction/oxidation process of the azobenzene group in the monolayer. The absence of bands for the C–H stretch of the methylene group and the N–H and C=O stretches of the amide moiety in the in-situ IRRAS spectra suggests that no orientation change occurs in the polymethylene chain of the monolayer during

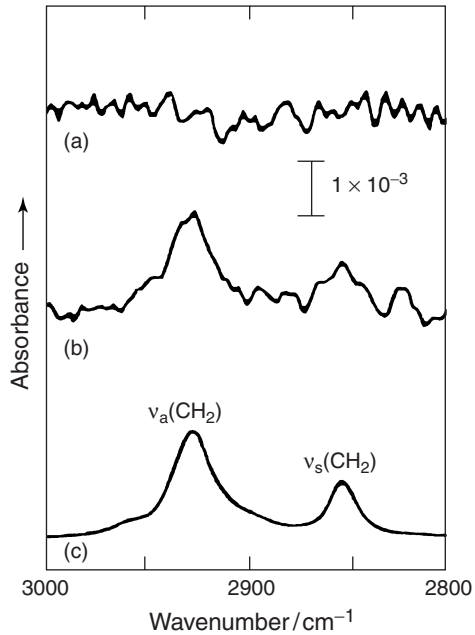

Figure 16. IRRAS spectrum showing the CH stretching region of (a) hexanedithiol (C_6) and (b) decanedithiol (C_{10}) SAMs. (c) Transmission spectrum of C10. [Reproduced by permission of the American Chemical Society from T. Nakanishi, B. Ohtani and K. Uosaki, *J. Phys. Chem. B,* **102**, 1571 (1998).]

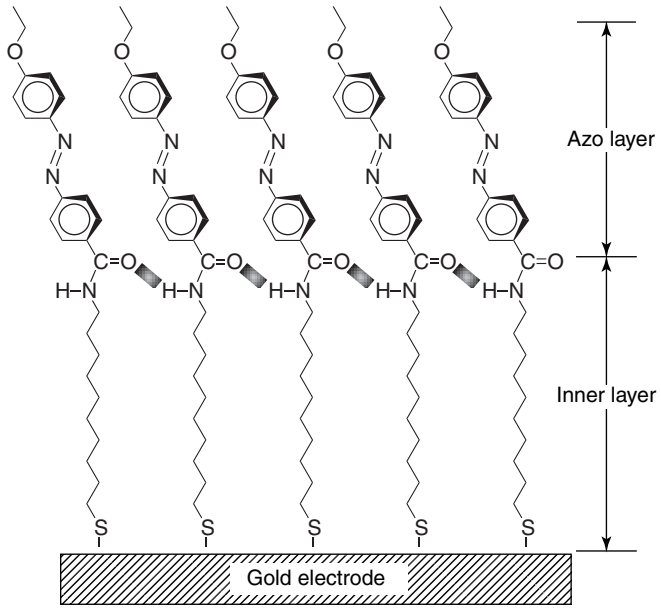

Figure 17. Schematic drawing of the $C_2AzoC_{10}SH$ SAM on the gold surface. [Reproduced by permission of the American Chemical Society from H.Z. Yu, H.L. Zhang, Z.F. Liu, S. Ye and K. Uosaki, *Langmuir,* **14**, 619 (1998).]

the redox reaction of the azobenzene group. The band intensity observed in the in-situ IRRAS spectra depends on the reaction time, especially in the reduction process of the azobenzene monolayer. Figure 18 gives the ratio of the

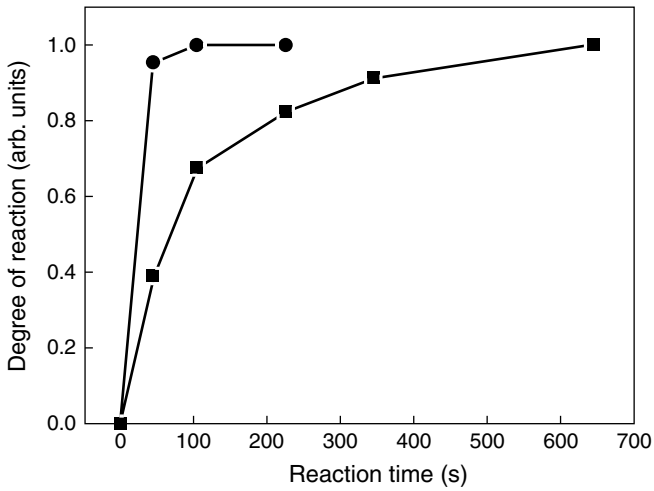

Figure 18. Hydrazobenzene to azobenzene ratio as a function of reaction for reduction (■) and re-oxidation (●). [Reproduced by permission of the American Chemical Society from H.Z. Yu, H.L. Zhang, Z.F. Liu, S. Ye and K. Uosaki, *Langmuir*, **14**, 619 (1998).]

hydrazobenzene to azobenzene as a function of the reaction time for the reduction and the reoxidation process.

These results provided direct evidence for a slower reduction of azobenzene to hydrazobenzene than the reverse process (i.e. the oxidation of hydrazobenzene), thus augmenting the importance of understanding the relationship between monolayer structure and electron transfer.

IRRAS was employed for the characterization of a "mixed" SAM using an asymmetrical spiroalkanedithiol, 2-octyl-2-pentadecylpropane-1,3-dithiol [$C_{10}C_{17}(SH)_2$], adsorbed onto gold.[14] The position of the antisymmetric methylene stretch $\nu_a^{CH_2}$ is commonly used to evaluate the crystallinity of organic thin films. In this study, the $\nu_a^{CH_2}$ band of the $C_{10}C_{17}(SH)_2$ SAM occurred at 2927 cm^{-1} which was higher that those of the SAMs prepared from either the symmetrical $C_{10}C_{10}(SH)_2$ or $C_{17}C_{17}(SH)_2$ (2925 cm^{-1} or 2921 cm^{-1}, respectively). For SAMs prepared from mixtures of varying ratios of n-$C_{10}SH$ and n-$C_{17}SH$, the position of this band was shifted from 2919 cm^{-1} (n-$C_{17}SH$) to a maximum of 2925 cm^{-1} for a 2–3 ratio of n-$C_{10}SH$/n-$C_{17}SH$. This was an indication of the similarity of the chemical composition of the SAMs.

Another area where IRRAS and PM-IRRAS were used extensively was for the study of thiol-based SAMs on gold.[15–20] Binary monolayers of varying ratios of mercaptopyrimidine (MP) and 1-dodecanethiol ($C_{12}SH$) were characterized.[21] Monolayers of several bidentate organosulfur compounds were characterized and compared to SAMs prepared from analogous alkanethiols.[22] Monolayers of decaneselenol[23] were found to adsorb onto gold similarly to alkanethiols. IRRAS was also used to probe SAMs of surfactants.[24] In addition, model structures for the study of

cell membranes consisting of a lipid monolayer over an alkanethiol monolayer were also characterized.[25]

Other applications of IRRAS include the determination of the tilt angles of 6-(10-mercaptodecaoxyl)quinoline (MDQ)[26] and azobenzene-containing alkanethiols[27,28] on Au and of the orientation of monolayers of amide containing alkanethiols[29] and alkanedithiols[30] on Au. Investigations of the ordering processes in chiral and racemic monolayers of three phenylalanyl-substituted O-thiol alkanoic acids on gold[31] were also reported.

Atomically flat, sputter-grown Au(111) films allowed well-ordered alkanethiol (exemplified by octanethiol) monolayers to be self-assembled from solution markedly faster and in larger domain sizes than previously reported.[32] The chain length of alkyl thiol tails tethering SAMs of phthalocyanine (Pc) derivatives to Au-coated optical waveguides was shown to have an effect on the orientation, packing density and intensity of observed fluorescence.[33] A very interesting study utilizes a chiral functionalized surface using SAMs of helical oligopeptides for intended application in molecular electronics, sensors and catalysis.[34]

In the area of SAMs grown on other substrates, contributions on the evaluation of SAM films, rod-like silylthiophene, silylbithiophene, and silylquaterthiophene derivatives on silicon oxide can be found.[35] IRRAS has also been used to study highly organized octadecylamine monolayers absorbed onto oriented films of $YBa_2Cu_3O_7$ (YBCO), a high Tc superconductor.[36] Furthermore, the formation of alkylsiloxane monolayers OxSi-$(CH_2)_n$-Y with different hydrocarbon chain lengths ($n = 10, 16, 17$) and different terminal substituents (Y = Me, COOMe, CN, Br) on native Si (Si/SiO_2) was studied by in-situ IRRAS.[37]

To study very fast dynamic processes at the electrochemical interface not readily accessible by conventional electrochemical techniques, a new dynamic IR spectroscopy was developed coupling step-scan Fourier transform infrared (FT-IR) interferometry, surface-enhanced infrared absorption spectroscopy (SEIRAS), and attenuated total reflection (ATR) techniques.[38] IRRAS verified charge transfer reactions between a SAM with charge-transfer functional groups and the complementary electron donor or acceptor.[39] These spectroscopic methods have also been applied to the effect of electrochemical potential on the structure of an octadecanethiol SAM.[40] SAMs of short chain ferrocenylalkyl disulfides with amide groups at various chain positions[41] were characterized by cyclic voltammetry and IRRAS. In-situ FT-IRRAS was used to monitor the potential dependent structural changes and decomposition of a 2-(11-mercaptoundecyl)hydroquinone SAM.[42]

The selective K^+ recognition (over Na^+, Cs^+, Ba^{2+}, and Ca^{2+}) during the formation of a SAM from a bispodand thiol on Au[43] has been reported. IRRAS was also used to measure specific binding interaction between the thiocarbohydrate SAMs and specific proteins.[44] The binding of a ferrocene-based cationic guest SAM with cyclodextrin was studied by IRRAS and electrochemical methods.[45] The adsorption of dimethyl methylphosphonate on alkanethiolate SAMs on gold[46] was also monitored.

3 INVESTIGATIONS OF LB FILMS

A brief description of the experimental considerations and history of LB films can be found elsewhere.[47] LB films are formed at the air–water interface. The process is initiated by spreading the substrate onto the surface of water in a Teflon® trough. A movable barrier is used to compress the molecules together to form a monolayer film at the air–water interface. A Wilhelmy plate is used as a feedback device, controlling the pressure on the film. The film can be studied in situ or be transferred to a substrate by dipping the substrate slowly through the air–water interface as the pressure on the film is held constant. The use of IR spectroscopy to evaluate structure–function relationships in LB films has been recently reviewed by Takenaka and Umemura.[48]

A very interesting study utilized LB films of regioregular poly(3-hexylthiophene) (RR-PHT) as field-effect transistors (FETs).[49] These LB films were stable at the air–water interface and could be transferred onto hydrophobic substrates by horizontal deposition. The LB films prepared by three different methods were characterized by ultraviolet–visible (UV–Vis) absorption spectroscopy, polarized visible absorption, X-ray diffraction, IRRAS, and field-effect mobility. Figure 19 shows the similarity of the IRRAS spectra of the three types of RR-PHT LB films.

In addition, Figure 20 shows a schematic structure of a FET fabricated from LB films of RR-PHT. The field-effect mobility of these FETs was among the highest of polymeric thin film LB FET devices.

In another study around LB films, the thermal property of octadecyldimethylamine oxide ($C_{18}DAO$) multilayer LB films was investigated by IRRAS and two techniques of molecular orientation analysis.[50] Figure 21 illustrates the IRRAS spectra of the $C_{18}DAO$ seven-monolayer LB film in the temperature range from 25 to 110 °C.

In addition to discussing the conventional theory for estimating molecular orientation, a modification of that theory was proposed to explain the temperature-dependent spectral changes. The results by the conventional analytical technique suggested that the multilayer LB film was thermally disordered at 50 °C and melted at 60 °C. The modified theory, on the other hand, suggested that only the first layer of the LB film is greatly disordered between 50 and 60 °C,

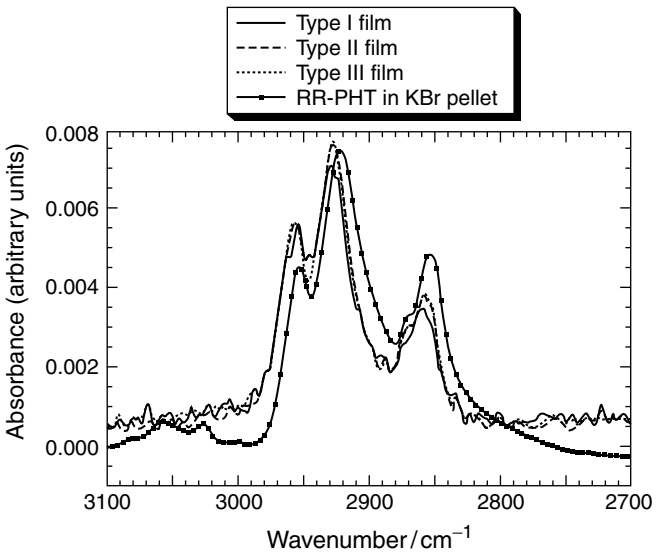

Figure 19. IRRAS spectra of the three types of LB films and the transmission spectrum of the bulk RR-PHT as a KBr pellet. [Reproduced by permission of the American Chemical Society from G. Xu, Z. Bao and J.T. Groves, *Langmuir*, **16**, 1834 (2000).]

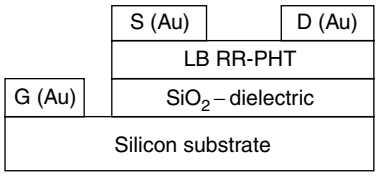

Figure 20. Schematic structure of the FET fabricated from RR-PHT films, showing the gate (G), the source (S) and the drain (D). [Reproduced by permission of the American Chemical Society from G. Xu, Z. Bao and J.T. Groves, *Langmuir*, **16**, 1834 (2000).]

prior to the total melting above 60 °C. This suggests that the LB film was not uniform but consisted of two distinguishable phases. The differing thermal properties of the first layer relative to the other layers suggested that the headgroup of C_{18}DAO with its strong dipole has a uniquely strong interaction potential with the gold surface.

Furthermore, monolayer and multilayers of ferroelectric liquid crystals (FLCs) obtained by the LB technique on the water subphase were characterized by surface pressure measurements and by PM-IRRAS.[51] The microscopic molecular organization of the films can be estimated by analysis of the PM-IRRAS spectra in terms of the specific surface selection rules for the film on the water surface. Figure 22 illustrates these surface selection rules that link the transition moment orientation with the sign and the intensity of the absorption band at the air–water interface.

The influence of the temperature on the structural arrangement of LB films was also discussed in Payan *et al.*[51] Specifically, Figure 23 shows the IR spectroscopic data at different temperatures from 22 °C up to 93 °C. The

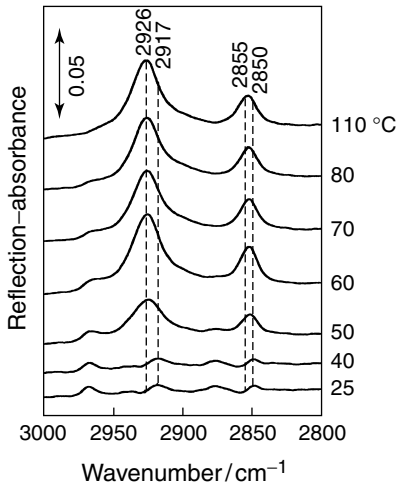

Figure 21. IRRAS spectra of the C_{18}DAO seven-monolayer LB film as a function of temperature. [Reproduced by permission of the American Chemical Society from T. Hasegawa, D.A. Myrzakozha, T. Imae, J. Nishijo and Y. Ozaki, *J. Phys. Chem. B*, **103**, 11 124 (1999).]

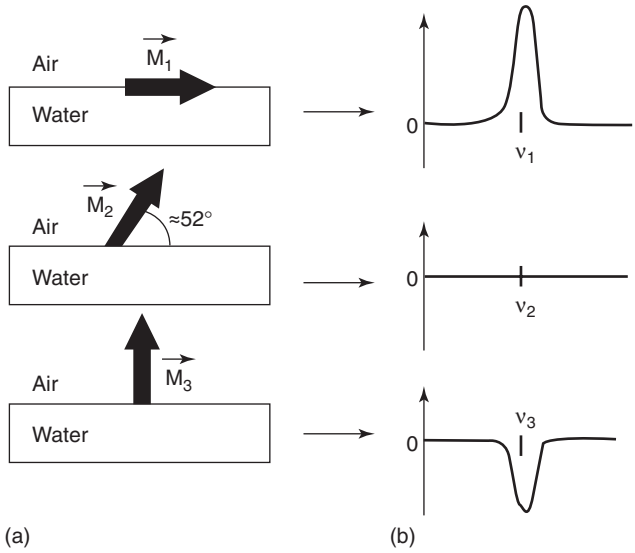

Figure 22. The surface selection rules at the air–water interface showing (a) the relationship between the transition moment orientation and (b) the intensity and sign of the absorption band. [Reproduced by permission of the American Chemical Society from S. Payan, B. Desbat, C. Destrade and H.T. Nguyen, *Langmuir*, **12**, 6627 (1996).]

dashed lines represent the phase transition of the bulk sample. It appears that the multilayer system has at least two phase transitions occurring at temperatures close to the observed transitions for the bulk material.

The photopolymerization process of the LB films of a diacetylene monocarboxylic acid, 10,12-pentacosadiynoic acid (DA) was studied using many techniques, among them IRRAS.[52] In particular, direct information about the conformation change of a polydiacetylene (PDA) that was

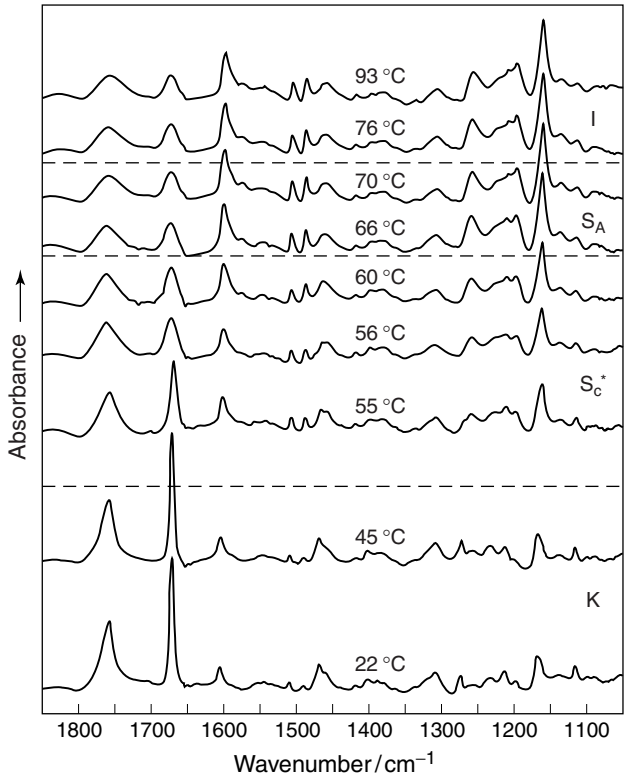

Figure 23. IR spectra of FLC-LB films on CaF_2 as a function of temperature. [Reproduced by permission of the American Chemical Society from S. Payan, B. Desbat, C. Destrade and H.T. Nguyen, *Langmuir*, **12**, 6627 (1996).]

produced by UV irradiation was obtained. The rate and extent of the polymerization of the cadmium salt of DA was monitored by the relative intensity change of the IRRAS signatures. The results established the mechanism of the conversion from a blue ($\lambda_{max} \sim 635$ nm) to a red phase ($\lambda_{max} \sim 540$ nm) during the polymerization of DA. The conversion proceeds through two steps. The polymerization reaction itself is almost completed in the first step, although a residual reaction may take place in the second step. The plane formed by the all-trans zigzag backbone of the alkyl groups changes its arrangement during the first step. The orientation of the long axis of the alkyl backbone changes from a tilted state to a less tilted one, keeping the axis perpendicular to the long axis within the plane parallel to the substrate surface. This orientation change is consistent with the observed increase in the interlayer spacing of the LB films of long-chain diacetylene monocarboxylic acids during their photopolymerization process. During the first step, the PDA backbone keeps a fully extended conformation with no interruption of conjugation and the formation of the blue phase proceeds. Throughout the second step, the regular plane of the all-trans alkyl group is converted to an irregular one containing gauche conformations. This conversion interrupts the fully extended backbone structure and reduces the average conjugation length, resulting in the formation of the red phase.

In another study, IRRAS was applied to study the structures and UV-light-induced photochemical processes of a cinnamic acid (CA) derivative (C22CA) in LB films on a silver substrate.[53] Figure 24 shows the structures of CA and C22CA and their photodimerization products.

For one to nine monolayer LB films of C22CA on silver substrate, the IRRAS spectra revealed that the frequency of the C=O and C=C bands varied as the surface pressure was changed from 10 to 30 mN m^{-1}. One-monolayer films prepared at 10–15 mN m^{-1} had bands at 1730 cm^{-1} ($\nu_{C=O}$) and at 1641 cm^{-1} ($\nu_{C=C}$), which are ascribed to a hydrogen-bonded chain of carboxyl groups or a lateral hydrogen-bonded state. However, the one-monolayer films prepared at higher surface pressures showed shifts of $\nu_{C=O}$ (1684–1674 cm^{-1}) and $\nu_{C=C}$ (1624 cm^{-1}) to lower frequencies, indicating the formation of cis hydrogen-bonded dimers. Films with three or more layers had bands at 1715 cm^{-1} ($\nu_{C=O}$) and 1639 cm^{-1} ($\nu_{C=C}$) which is indicative of hydrogen bonding between the adjacent monolayers or face-to-face hydrogen bonding. Figure 25 depicts the structures of the cis and trans hydrogen-bonded dimers.

UV irradiation of the one-monolayer films prepared at low surface pressure does not afford any changes in the IRRAS spectra. However, there are quite dramatic changes in the IRRAS spectra of one-monolayer films prepared

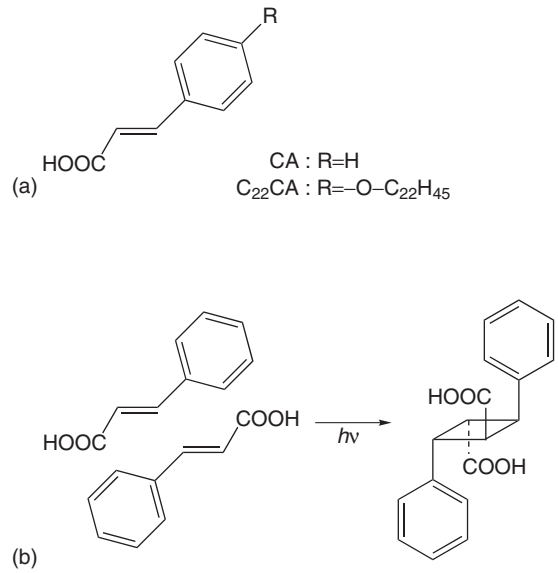

Figure 24. (a) Structures of CA and C22CA and (b) the photodimerization reaction. [Reproduced by permission of the American Chemical Society from M. Yamamoto, N. Furuyama and K. Itoh, *J. Phys. Chem.*, **100**, 18 483 (1996).]

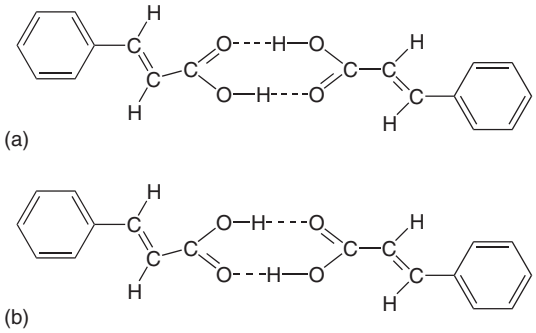

Figure 25. Structures of (a) the cis and (b) the trans hydrogen-bonded dimers of CA. [Reproduced by permission of the American Chemical Society from M. Yamamoto, N. Furuyama and K Itoh, *J. Phys. Chem.*, **100**, 18 483 (1996).]

at higher surface pressure. Figure 26 reveals the spectral changes during UV irradiation of these one-monolayer C22CA films. Thus, the cis hydrogen-bonded C22CA dimers undergo photodimerization, but the molecules in the lateral hydrogen-bonded state do not.

IRRAS investigations of the multilayered films also revealed that the irradiation causes the conversion from the face-to-face hydrogen-bonded state to an irregular state consisting of the lateral hydrogen-bonded state and a non-hydrogen-bonded state. The conversion to the trans hydrogen-bonded dimer caused by the thermal treatment and the conversion to the irregular state due to the irradiation indicate that the face-to-face hydrogen bonded state is thermodynamically in a metastable (or a kinetically trapped) state. The utility of IRRAS in establishing the relationship between the structures of the C22CA LB films and the photochemical processes was clearly demonstrated.

A subsequent work on photodimerization processes induced by UV-light irradiation of LB films of a stilbazole derivative ($C_{18}S$) or a diaryl-1,3-butadiene ($C_{18}B$) embedded in fully deuterated arachidic acid (DAA) on a silver substrate[54] also employed IRRAS. Figure 27 depicts the structure and possible photodimerization products of these materials and the trans CA derivative C22CA for reference. LB films of fully deuterated DA incorporating $C_{18}S$ or $C_{18}B$ in ratios of 1 : 4 ($C_{18}S$ or $C_{18}B$: DA) were reported. Other films were prepared using a 1 : 9 ratio of the incorporated $C_{18}S$ or $C_{18}B$ to DAA in either acid or salt forms.

Examination of the spectral changes observed during UV irradiation of the $C_{18}S$ film revealed that the cis cyclobutane ring is formed initially in the photoprocess, followed by the appearance of the trans form as the irradiation continues. For the $C_{18}B$ films, the photoprocess results in the formation of a cyclobutane ring rather than the cyclo-octadiene ring. Kinetic information about the photodimerization process was also obtained from the IRRAS spectra. Figure 28 shows the spectral changes induced by UV irradiation of the $C_{18}S$ and $C_{18}B$ films.

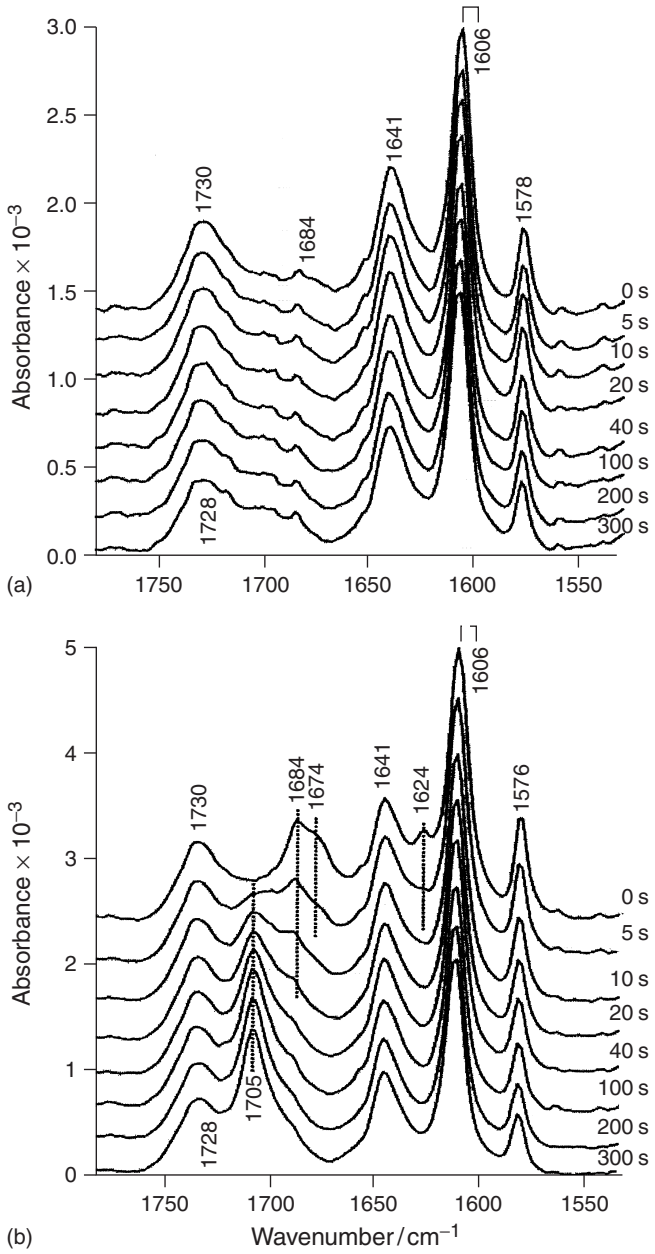

Figure 26. IRRAS spectral changes during UV irradiation of one-monolayer films of C22CA. (a) Film prepared at $10\,mN\,m^{-1}$. (b) Film prepared at $30\,mN\,m^{-1}$. [Reproduced by permission of the American Chemical Society from M. Yamamoto, N. Furuyama and K. Itoh, *J. Phys. Chem.*, **100**, 18 483 (1996).]

In another photochemical study, polychromic nine-layer LB films consisting of polyion complexes of 4-octyl-4′-(5-carboxypentamethyleneoxy)azobenzene (8A5) and stearic acid-d35 (St-d35) with polyallylamine have been prepared.[55] IRRAS was used to study the orientational regulation of St-d35 by trans–cis photoisomerization of 8A5 in these LB films. Intensity changes in CH_2, benzene ring, ϕ-O and ϕ-N bands of the alkyl chain and azobenzene portions of 8A5 are indicative of the cis–trans isomerization.

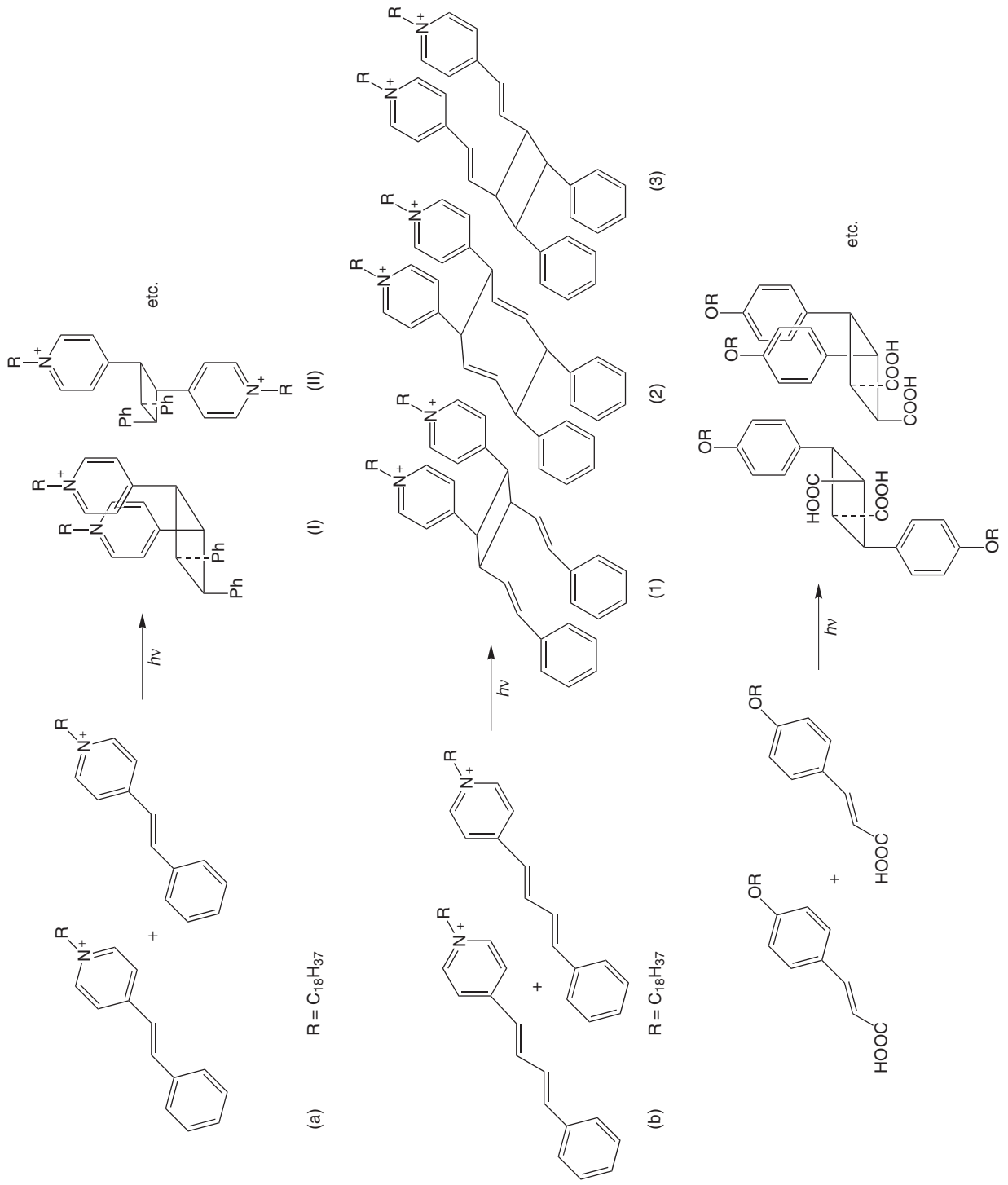

Figure 27. The possible photodimerization products of (a) $C_{18}S$, (b) $C_{18}B$ and (c) C22CA. [Reproduced by permission of Springer from K. Itoh, M. Yamamoto, N. Furuyama and A. Saito, 'Infrared Reflection Absorption Spectroscopic Study on Photochemical Processes in Langmuir–Blodgett Films', in "Progress in Fourier Transform Spectroscopy", eds J. Mink, G. Keresztury and R. Kellner, Springer-Verlag, Vienna, Austria, 33–42 (1997).]

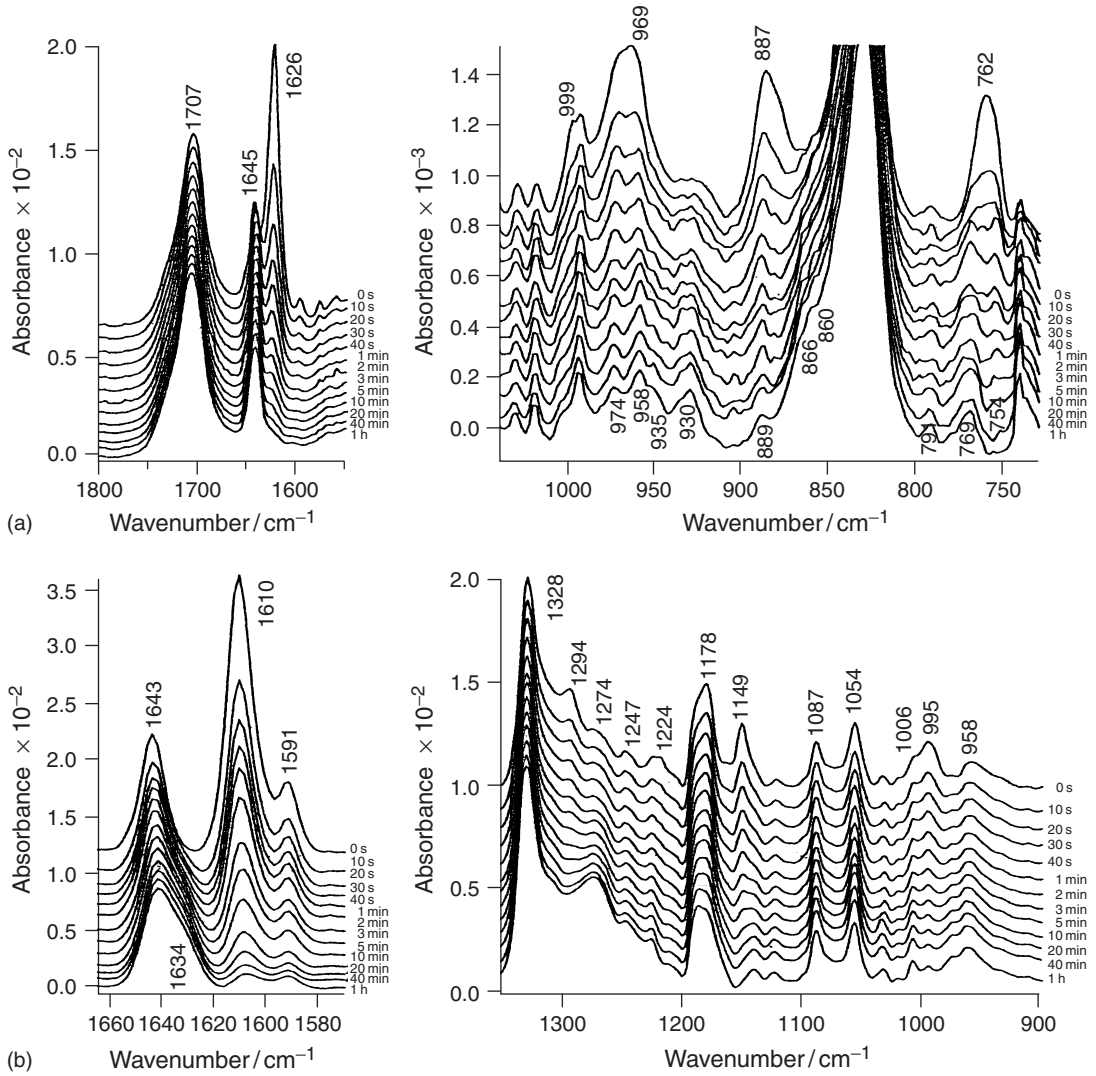

Figure 28. Changes in the IRRAS spectra for (a) $C_{18}S$ and (b) $C_{18}B$ in LB films of DA during UV-irradiation at 340 nm and 370 nm, respectively. [Reproduced by permission of Springer from K. Itoh, M. Yamamoto, N. Furuyama and A. Saito, 'Infrared Reflection Absorption Spectroscopic Study on Photochemical Processes in LB Films', in "Progress in Fourier Transform Spectroscopy", eds J. Mink, G. Keresztury and R. Kellner, Springer-Verlag, Vienna, Austria, 33–42 (1997).]

Changes in the CD_2 and COO^- stretching bands of St-d35 are used to monitor orientational changes in St-d35. The IRRAS spectra show that irradiation with UV light between 45 and 65 °C leads to an orientation change in St-d35 by 8A5 isomerization, and that irradiation with visible light re-establishes the initial conditions. Figure 29 shows the spectral changes associated with this isomerization at 55 °C.

However, this orientation process is strongly temperature dependent. The photoregulation of the orientation of St-d35 is considerably lessened below 35 °C and above 75 °C. Figure 30 displays the spectral changes at 25 °C.

Finally, IR and IRRAS were used to investigate the structure, orientation and phase transitions of LB films of an amphiphilic polymer.[56] This material (ES-3) consists of a microgel portion, which is a flexible slightly crosslinked epichlorohydrin–ethylenediamine network, and hydrophobic stearic grafting chains. The IR study indicates that the LB films of ES-3 possess crystalline, tightly packed methylene chains and extended interchain hydrogen bonds between the amide groups, which connect the alkyl chains with the microgel. ES-3 forms a monolayer with a "reversed duckweed" structure as shown in Figure 31 where the grafting chains point away from the water surface.

Using the surface selection rules, comparison of the band intensities between transmission and reflection-absorption spectra suggests that the hydrocarbon chains are almost perpendicular to the substrate and that N–H and C=O bonds of the amide groups are nearly parallel to the surface as are the interchain hydrogen bonds between the N–H and C=O bonds. Studies of the LB films of ES-3 prepared under

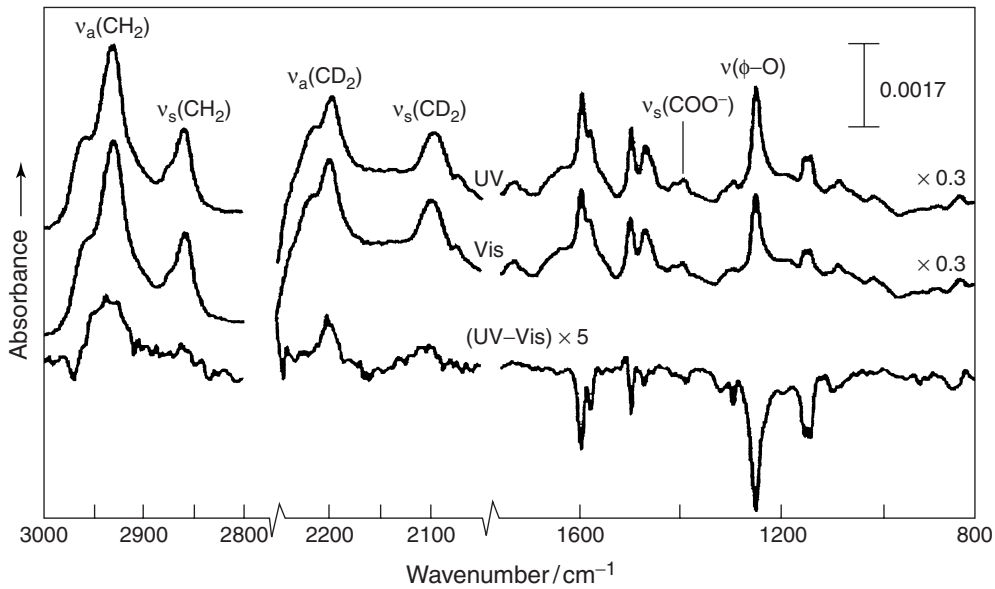

Figure 29. Spectral changes observed for the nine-monolayer 8A5+St-d35/PAA film under visible or UV-irradiation at 55 °C. [Reproduced by permission of the American Chemical Society from T. Kawai, *J. Phys. Chem. B*, **103**, 5517 (1999).]

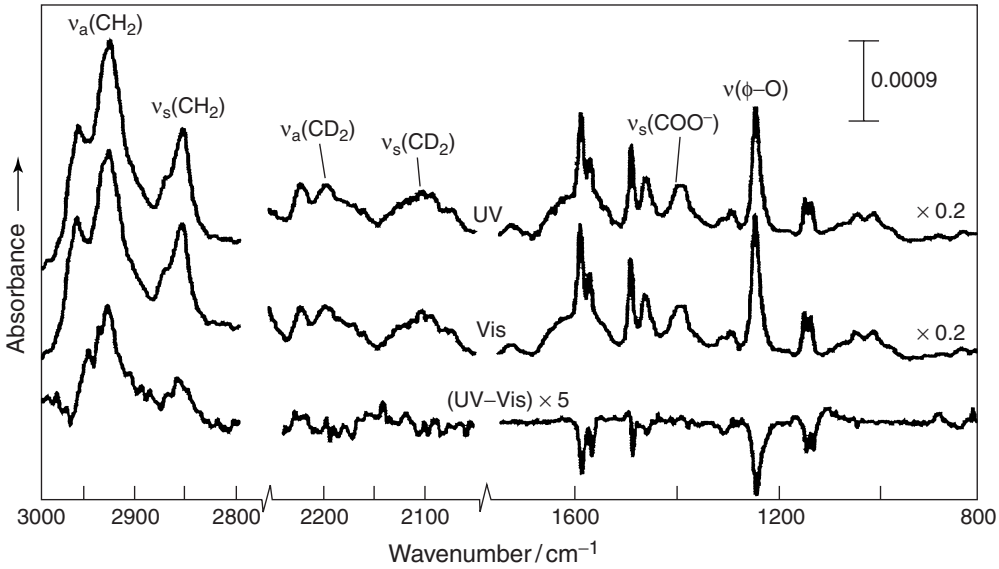

Figure 30. Spectral changes observed for the nine-monolayer 8A5+St-d35/PAA film under visible or UV-irradiation at 25 °C. [Reproduced by permission of the American Chemical Society from T. Kawai, *J. Phys. Chem. B*, **103**, 5517 (1999).]

different surface pressures indicate that the alkyl chains are highly ordered even in the film deposited under nearly zero surface pressure. Multilayer LB films of ES-3 show three sharp phase transitions near 65, 105 and 140 °C. This is in contrast to self-assembled films of ES-3, which show only two transitions. This behavior may be explained by the partial interdigitation of the alkyl chains of the self-assembled film versus the LB film, which shows no interdigitation. Figure 32 presents the temperature dependence of the frequency (●) and band width (▲) at half the peak height for the CH_2 antisymmetric stretching band for two LB films having eleven layers and one layer, respectively.

Even the one-monolayer LB film of ES-3 shows clear phase transitions in contrast to LB films of low molecular weight organic dyes, which do not give sharp phase transitions. It is likely that the microgels inhibit direct interaction between the substrate and the alkyl chains in the first layer.

A number of other recent studies, which utilized IRRAS, are noted below. IRRAS was used in the study of LB films

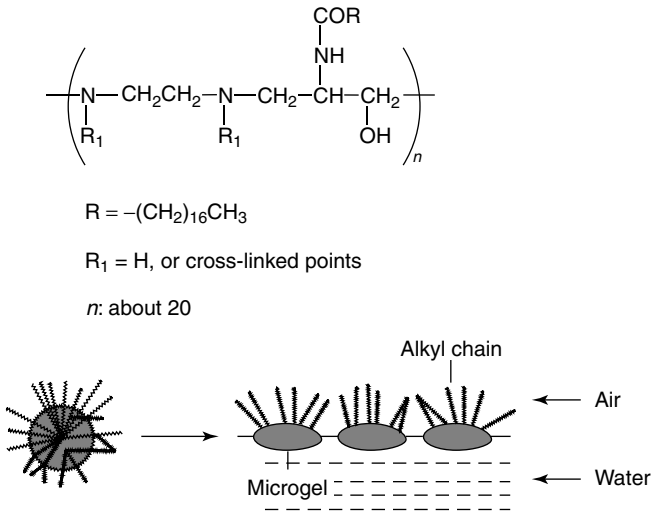

Figure 31. Schematic of the "reversed duckweed" monolayer on the water subphase and the structure of the ES-3 amphiphilic polymer. [Reproduced by permission of the American Chemical Society from B. Zhao, H. Li, X. Zhang, J. Shen and Y. Ozaki, *J. Phys. Chem. B*, **102**, 6515 (1998).]

of a crosslinkable polymer[57] for high resolution patterning and of methacrylamide copolymers for a water developable positive photoresist.[58] The LB films of several charge transfer materials[59,60] were also studied. Two-monolayer LB films, consisting of barbituric acid (BA) and triaminotriazine (TAZ) derivatives (C18BA and 2C18TAZ) deposited at various surface pressures on a gold-evaporated substrate covered with a deuterated cadmium stearate (CdSt-d35) monolayer, were measured by IRRAS to investigate the hydrogen-bonding network formed between the two layers.[61]

The dependence of orientation and structure on the substrate, aging and pH of the water subphase has also been studied.[62] Aggregation and orientation properties of LB films of 1-hydroxy-5-hexadecyloxynaphthalene[63] and of mixed LB films of 5-(4-*N*-octadecylpyridyl)-10,15,20-tri-*p*-tolylporphyrin and stearic acid[64] were measured. The change in orientation of an 11-ferrocenyl-1-undecanethiol SAM on gold induced by redox reaction of the ferrocenyl group was examined.[65]

4 INVESTIGATION OF THIN POLYMER FILMS

Horn[66] has recently reviewed IRRAS techniques for the study of thin interfacial films. IRRAS of monolayers formed at the air–water interface has been reviewed.[67] A review of the applications and characteristics of photon-in, photon-out optical techniques, including IRRAS, used to characterize organic thin solid films and their interfaces was

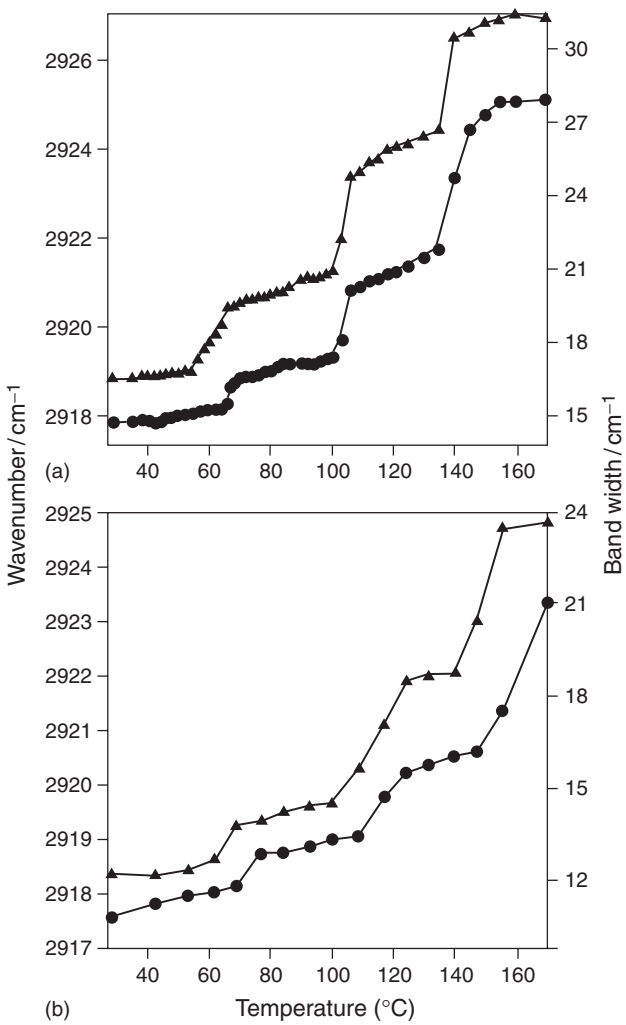

Figure 32. Temperature dependence of the CH_2 antisymmetric stretching band of (a) eleven-layer and (b) one-layer ES-3 LB films. Band width is determined at half peak height. [Reproduced by permission of the American Chemical Society from B. Zhao, H. Li, X. Zhang, J. Shen and Y. Ozaki, *J. Phys. Chem. B*, **102**, 6515 (1998).]

published.[68] A general review of spectroscopic methods for the characterization of thin organic and polymeric films[69] and a review of Raman and IR spectroscopy of layered structures[70] should be noted.

In a very interesting study, the photo-oxidative stability of two electroluminescent polymers, poly(2,5-bis(cholestanoxy)-1,4-phenylene vinylene) (BCHA-PPV) and poly(3-octylthiophene) (P3OT) on Au and Al substrates, was determined.[71] The photo-oxidation of the thin polymer films was analyzed in situ using IRRAS. Ex-situ characterization of the films employed X-ray photoelectron spectroscopy (XPS) and attenuated total reflection infrared (ATR-IR) spectroscopy. Figure 33 presents the IRRAS spectra of 400 Å thick BCHA-PPV films on Au and Al before and after UV irradiation.

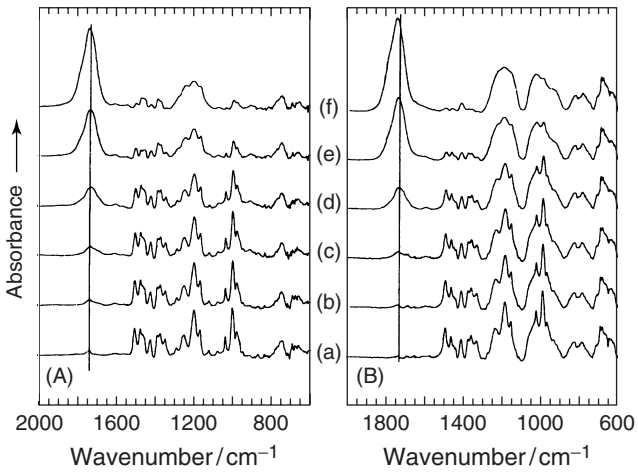

Figure 33. IRRAS spectra of 400 Å films of BCHA-PPV on (A) Au and (B) Al, showing (a) the as-coated films and spectra as a function of UV-irradiation in dry air for (b) 2, (c) 5, (d) 12, (e) 24 and (f) 36 h. [Reproduced by permission of Elsevier from B.H. Cumpston and K.F. Jensen, *Synth. Met.*, **73**, 195 (1995).]

The oxidation of BCHA-PPV is quite extensive, as evidenced by the appearance of a carbonyl band at 1723 cm^{-1} that increases in intensity and shifts to 1737 cm^{-1} at longer UV exposure times. This and other changes in the spectra implicate the formation of an ester and volatile aldehyde species. In contrast, P3OT shows no detectable oxidation during similar exposure. Figure 34 depicts the proposed photo-oxidation mechanism of BCHA-PPV involving singlet oxygen derived from energy transfer from the BCHA-PPV triplet state. The energy levels for BCHA-PPV and molecular oxygen are illustrated in Figure 35.

Because the singlet exciton state is responsible for luminescence in the film, BCHA-PPV triplet exciton states will also form during electroluminescent device operation. This will result in the formation of reactive singlet oxygen. Thus, it appears that BCHA-PPV will slowly self-degrade in the presence of oxygen when used as the active layer in such devices.

Other applications to thin polymer films include the characterization of the molecular structure of thin polystyrene and polyethylene films following low-pressure plasma treatment.[72] A series of papers[73–76] have focused on the characterization of various bisperylene films using IRRAS and Raman spectroscopic techniques. In-situ PM-IRRAS studies of imidazole films electrochemically deposited on copper determined the amount of imidazole bound to the copper electrode and its orientation.[77] PM-IRRAS was employed to investigate in situ the conformations and orientations of peptides bound to dimyristoyl-phosphatidylcholine.[78] The orientation of vinylidene fluoride oligomer formed by evaporation was characterized.[79] The surface modification of carbon electrodes by electrochemical reduction of aromatic diazonium salts was probed by a variety of techniques including IRRAS.[80]

A multilayer film consisting of alternating layers of poly(L-lysine) and poly(L-glutamic acid) adsorbed onto carboxylic acid terminate alkanethiol modified gold surfaces is capable of binding electroactive materials such as ferri/ferrocyanide. PM-IRRAS was used to characterize the film, monitor the incorporation of electroactive species and to study the effects of electrochemical oxidation of the ferrocyanide to ferricyanide.[81]

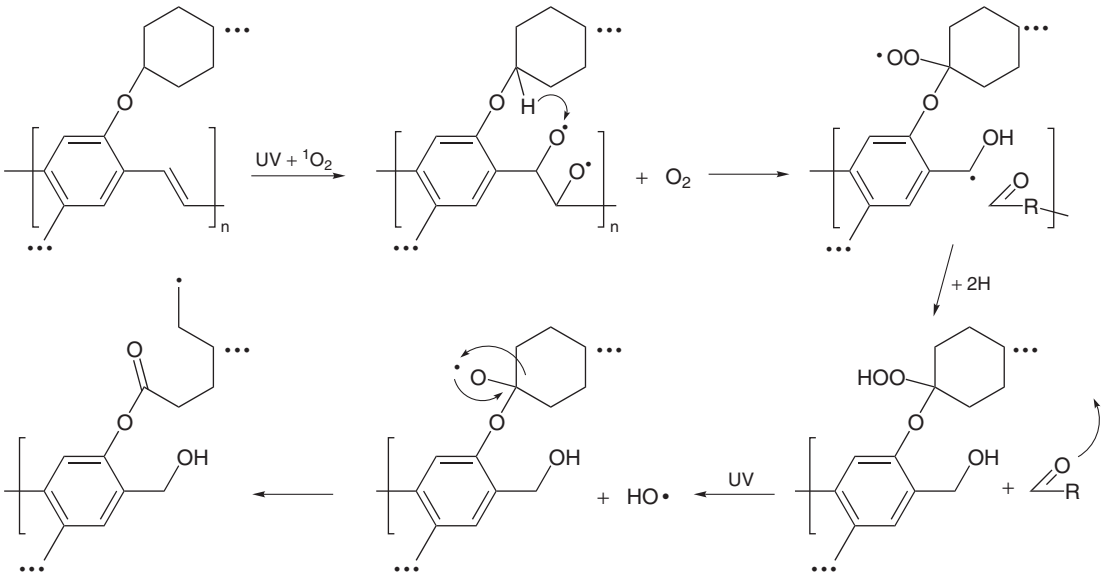

Figure 34. The proposed mechanism for the photo-oxidation of BCHA-PPV. [Reproduced by permission of Elsevier from B.H. Cumpston and K.F. Jensen, *Synth. Met.*, **73**, 195 (1995).]

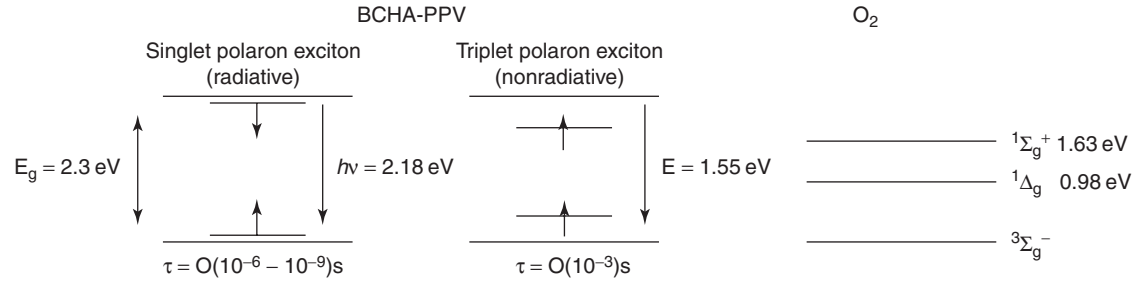

Figure 35. Energy levels for BCHA-PPV and molecular oxygen. For comparison, the ground state of oxygen and the polymer valence band levels are fixed at 0.0 eV. [Reproduced by permission of Elsevier from B.H. Cumpston and K.F. Jensen, *Synth. Met.*, **73**, 195 (1995).]

PM-IRRAS has been used to investigate properties of various thin films at the air–water interface.[82] In-situ PM-IRRAS was utilized to characterize the films formed by two methods of preparing monolayers of photosystem II core complex.[83,84] Investigations of the orientation of bacteriorhodopsin monolayers was also reported.[85] Several studies on phospholipids,[86–88] acetylcholinesterase,[89] cellulose,[90,91] and alcohol monolayers[92] have been published. The orientation of a cyanobiphenyl liquid crystal in both Langmuir films and freely suspended films was investigated.[93] The molecular structure and orientation of a 1 : 1 hydrogen-bonding network formed between a TAZ amphiphile (2C18TAZ) and complementary BA at the air–water interface was studied.[94] The NH_2 scissoring band and ring quadrant stretch absorption bands of the 2C18TAZ molecule were used to characterize the interaction.

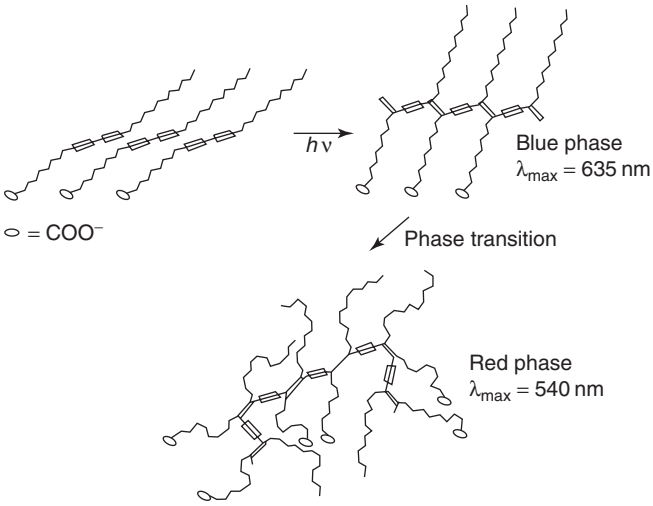

Figure 36. Schematic diagram of the photopolymerization of the diacetylene LB films. [Reproduced by permission of the American Chemical Society from E. Shirai, Y. Urai and K. Itoh, *J. Phys. Chem. B*, **102**, 3765 (1998).]

5 RAMAN STUDIES

A number of very interesting studies where surface-enhanced resonance Raman scattering (SERRS) spectroscopy was utilized have appeared recently in the literature. In one such study, the photopolymerization of a one-layer LB film of the cadmium salt of DA, a diacetylene monocarboxylic acid derivative, on a 60 Å thick evaporated silver island film was studied by SERRS.[95] Figure 36 shows the polymerization mechanism for a multilayer LB film ($L \geq 3$) on a smooth silver substrate with a mass thickness of 1000 Å. The initial step is the formation of a blue phase ($\lambda_{max} = 635$ nm) having a regular trans zigzag structure to a red phase ($\lambda_{max} \approx 540$ nm) which is an irregular orientation containing gauche conformations.

The resonance Raman scattering spectra of a 15-layer LB film of DA (Figure 37) shows the shift of the $\nu_{(C\equiv C)}$ and $\nu_{(C=C)}$ bands. The $\nu_{(C\equiv C)}$ band envelope can be resolved into three distinct bands with the band at 2083 cm^{-1} assigned to the blue phase and the band at 2111 cm^{-1} assigned to the irregular red phase. The band at 2095 cm^{-1} may be assigned to a phase of intermediate conjugation length. Figure 38 shows the relative intensities of these three bands versus irradiation time, demonstrating the rapid formation of the blue phase, followed by the subsequent formation of the red phase.

As shown in Figure 39, the photopolymerization of the monolayer film on the surface-enhanced Raman scattering (SERS)-active 60 Å silver substrate was found to proceed much faster than that on the smooth (SERS-inactive) substrate ($d = 1000$ Å). The similarity of the curves in Figure 40 to the curves in Figure 38 indicates that the monolayer undergoes photopolymerization as well as the blue-to-red phase transition.

The rate of the photopolymerization of the monolayer on the island film was greater than for series of LB films of DA on silver films with $d = 60–1000$ Å. In addition, the increase of the distance between the reacting monolayer and the 60 Å silver substrate by adding spacer layers of LB films of arachidic acid, decreased the relative intensity of the $\nu_{(C\equiv C)}$ bands. Both results are characteristic features

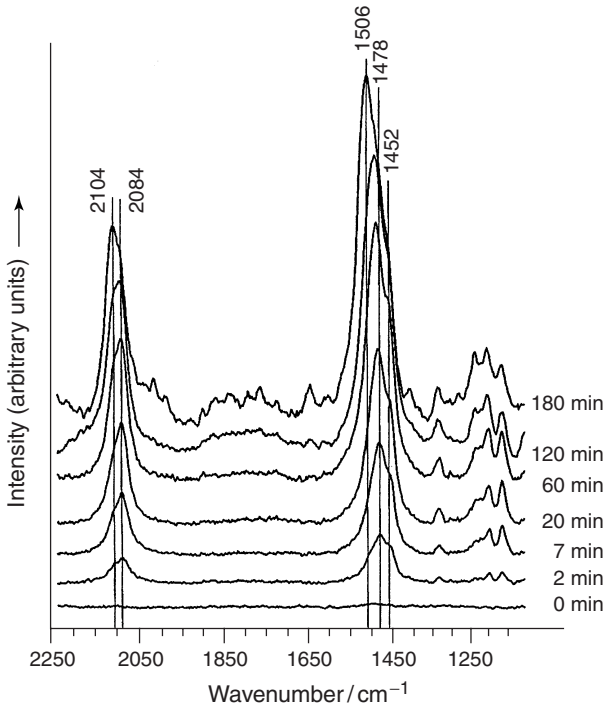

Figure 37. Resonance Raman spectra for the photopolymerization of the 15-layer LB film on the 1000 Å silver film. Irradiated at 552 nm. Time is shown on the right. [Reproduced by permission of the American Chemical Society from E. Shirai, Y. Urai and K. Itoh, *J. Phys. Chem. B*, **102**, 3765 (1998).]

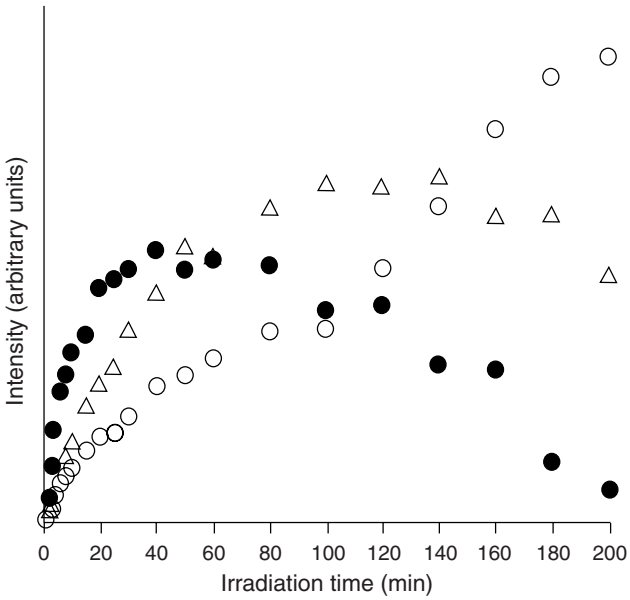

Figure 38. Intensity changes of the three-component bands as a function of irradiation time: (●) 2083 cm^{-1}; (○) 2111 cm^{-1}; (△) 2095 cm^{-1}. [Reproduced by permission of the American Chemical Society from E. Shirai, Y. Urai and K. Itoh, *J. Phys. Chem. B*, **102**, 3765 (1998).]

of the SERS effect. The rate enhancement is due to an addition reaction of DA to reactive PDA oligomers,

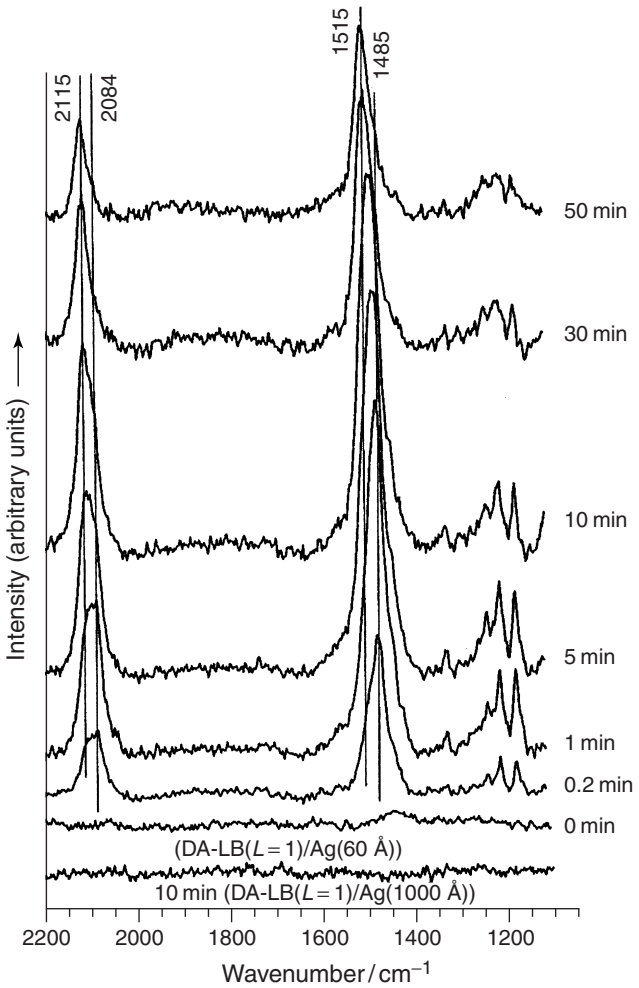

Figure 39. Comparison of the SERRS spectra for the one-monolayer LB film on the 60 Å silver as a function of irradiation time with the RRS spectrum (bottom trace) of the one-monolayer film on the 1000 Å Ag surface. The films were irradiated at 532 nm. [Reproduced by permission of the American Chemical Society from E. Shirai, Y. Urai and K. Itoh, *J. Phys. Chem. B*, **102**, 3765 (1998).]

resulting from an enhanced band-to-band transition of the oligomers caused by a strong coupling of the transition to the localized plasmon resonance of the substrates.

Another interesting study focused on the photopolymerization of diacetylenes as SAMs.[96] Resonance Raman spectroscopy was used to study a diacetylene disulfide monomer, dinonacosa-10,12-diyn-disulfide (15,9-DA), on a gold surface on a mica substrate. The monomer is attached to the gold surface via the S moiety. As shown in Figure 41, polymerization of one of the diacetylene species leads to formation of the backbone parallel to the surface.

Figure 42 illustrates that the initial formation of the blue polymer form, indicated by the increase in intensity of bands at 1459 and 2082 cm^{-1}, was followed by irreversible

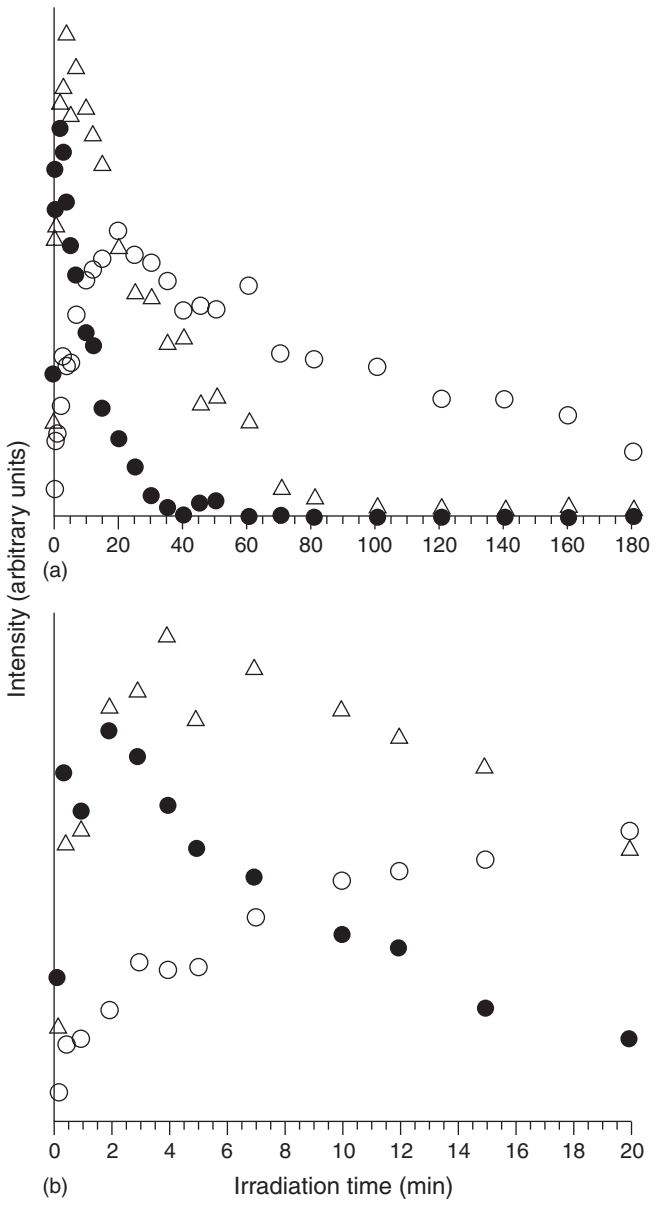

Figure 40. Relative intensity changes of the component bands as a function of irradiation time: (a) 0 to 180 min; (b) 0 to 20 min. Band identifiers: (●) 2083 cm^{-1}; (○) 2111 cm^{-1}; (△) 2095 cm^{-1}. [Reproduced by permission of the American Chemical Society from E. Shirai, Y. Urai and K. Itoh, *J. Phys. Chem. B*, **102**, 3765 (1998).]

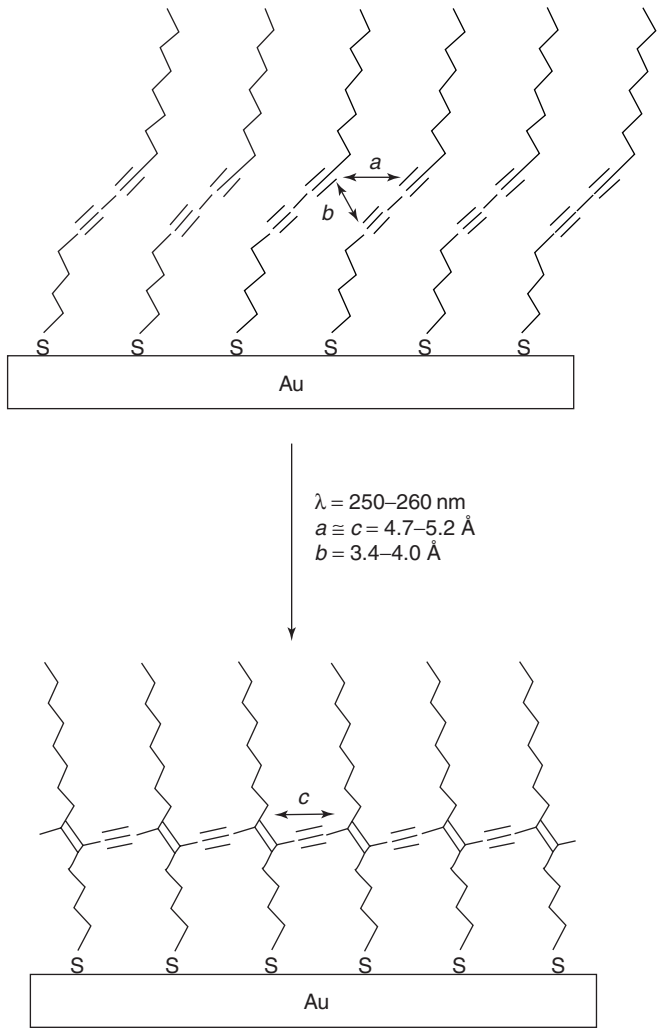

Figure 41. Schematic diagram of the spatial constraints of the polymerization. [Reproduced by permission of the American Chemical Society from M. Cai, M.D. Mowery, H. Menzel and C.E. Evans, *Langmuir*, **15**, 1215 (1999).]

loss upon prolonged UV exposure. This behavior mirrors the chromatic phase transition to shorter conjugation lengths exhibited for multilayer LB films upon extended UV exposure. Theories on the nature of this phase transition focus on factors that affect the alignment of the polymer backbone and influence the effective conjugation length. Three such factors were considered. The polymerization process did not induce any cleavage of the Au–S bond with the surface. Although no change in chain crystallinity was seen upon polymerization, the twist of the methylene chain exhibited significant changes with prolonged UV exposure. This is consistent with the hybridization-induced strain being translated into the polymer backbone and the methylene chains, resulting in a decrease in the effective conjugation length.

In addition, Raman spectroscopy has been used to characterize octadecyltrichlorosilane and dimethylchlorooctadeclsilane covalently bonded to modified silver surfaces.[97] Chromatic phase properties of diacetylene SAMs on gold were studied by dual-wavelength laser excitation resonance Raman.[98] Monolayer contamination of C_nSH and $C_8D_{17}SH$ SAMs by a small polyaromatic hydrocarbon was determined.[99] The study of a homologous series of sodium dialkylsulfosuccinates showed that the C=O and SO_3 stretch modes reflect the interaction between headgroup and counterion.[100]

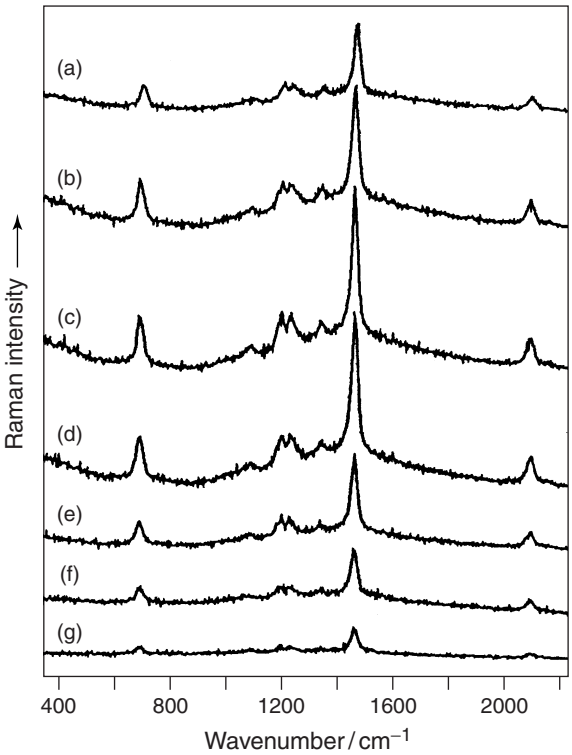

Figure 42. Resonance Raman spectra of 15,9-DA on Au surfaces. UV exposure under nitrogen for (a) 2, (b) 4, (c) 7, (d) 12, (e) 33, (f) 53 and (g) 93 min. [Reproduced by permission of the American Chemical Society from M. Cai, M.D. Mowery, H. Menzel and C.E. Evans, *Langmuir*, **15**, 1215 (1999).]

The effect of electrochemical oxidation and reduction on the orientation of anthraquinonylbutylsulfide SAMs on silver and gold electrodes was investigated by SERS.[101] The mechanism of the UV photo-oxidation of alkanethiol SAMs[102] was determined. Surface Raman spectroscopy was used to study the effects of electrolyte and applied potential on the formation of *n*-alkanethiol SAMs on gold.[103] The complexation of optically active azo dyes with thiolated cyclodextrin SAM was followed by monitoring characteristic vibrations of the dye molecules.[104] Surface-enhanced Raman imaging was used to obtain a two-dimensional image of a photopatterned *p*-nitrothiophenol SAM on silver.[105] Polymerization of variously terminated alkanethiols on gold[106] and (mercaptomethyl)-styrene[107] was studied by SERS.

SERS and IRRAS were used to study SAMs prepared from viologen derivatives.[108] Alkanethiols on poly crystalline gold[109] and on mechanically polished smooth silver and gold surfaces[110] were examined. A detailed Raman and SERS study of monolayers of p-substituted benzenethiols and benzenemethanethiols on gold electrodes[111] was reported. SERS was used to investigate the structure and thermal stability of SAMs of diselenides and disulfides.[112] The feasibility of using selenolates as alternatives to thiolates was investigated by SERS.[113]

The use of SERS in the characterization of LB films of poly(*o*-methoxyaniline),[114] imidazole-coordinated metal complexes,[115] amphiphilic nitroaniline derivatives such as *n*-docosyl-2-Me-4-nitroaniline (DCMNA)[116] and C60 monolayers[117] has also been recently reported. IRRAS and SERS were used for the characterization of polyimide LB films on silver,[118] and for orientation studies of LB monolayers of perylenetetracarboxylic anhydrides[119] and diimides.[120] A novel fiber-optic interface was developed for Raman spectroscopy of supported monolayers.[121] Thin organic films of copper Pc, fullerene or perylene derivatives incorporating metal clusters of silver, gold or copper have been studied by SERS.[122,123] Finally, resonance Raman and surface-enhanced resonance Raman were used to study polymer-modified electrodes which mimic heme enzymes.[124]

In conclusion, the use of vibrational spectroscopy for the study of thin organic films will acquire even more significance in the years to come. This is due to the fact that we are moving fast towards miniaturization and nanotechnology in general. Therefore, the demand for the use of analytical methods that give both the chemical composition and molecular orientation of very thin films at surfaces will be high. We expect to see many new and very interesting applications of the above-mentioned techniques in the near future.

ABBREVIATIONS AND ACRONYMS

AOT	Aerosol OT
ATR	Attenuated Total Reflection
ATR-IR	Attenuated Total Reflection Infrared
AZO	4,4′-Azodibenzenediylbis(phosphonate)
BA	Barbituric Acid
BCHA-PPV	Poly(2,5-bis(cholestanoxy)-1,4-phenylene vinylene)
CA	Cinnamic Acid
CdS	Cadmium Sulfide
$C_{18}B$	Diaryl-1,3-butadiene
$C_{18}DAO$	Octadecyldimethylamine Oxide
$C_{18}S$	Stilbazole Derivative
$C_{12}SH$	1-Dodecanethiol
DA	10,12-Pentacosadiynoic Acid
DAA	Deuterated Arachidic Acid
DBAzC10	4,4′-[(1,12-dioxo-1,12-dodecanediyl)-diimino]bisbenzoyl Azide
DBP	1,10-Decanediylbis(phosphonate)
DCMNA	*n*-docosyl-2-Me-4-nitroaniline
DCV	Dansylcadaverine

DMT	Dimethoxytrityl
ECz	*N*-ethylcarbazolyl
EDTA	Ethylenediaminetetraacetic Acid
FET	Field-effect Transistor
FLC	Ferroelectric Liquid Crystal
Fmoc	9-Fluorenyl-Methoxy-Carbonyl
FT-IR	Fourier Transform Infrared
HAPA	[5-[4-[4-[[(6-Hydroxyhexyl)sulfonyl]-phenyl]azo]phenyl]pentoxy]phosphonic Acid
IRRAS	Infrared Reflection-Absorption Spectroscopy
LB	Langmuir–Blodgett
MDQ	6-(10-Mercaptodecaoxyl)quinoline
MP	Mercaptopyrimidine
MUAM	11-Mercaptoundecylamine
MUD	11-Mercaptoundecanol
NHS	*N*-hydroxysuccinimide
PAAm	Poly(allylamine hydrochloride)
Pc	Phthalocyanine
PDA	Polydiacetylene
PM	Polarization Modulation
PM-IRRAS	Polarization Modulation Infrared Reflection-Absorption Spectroscopy
P3OT	Poly(3-octylthiophene)
RR-PHT	Regioregular Poly(3-hexylthiophene)
SAM	Self-assembled Monolayer
SEIRAS	Surface-enhanced Infrared Absorption Spectroscopy
SERRS	Surface-enhanced Resonance Raman Scattering
SERS	Surface-enhanced Raman Scattering
SHG	Second Harmonic Generation
SPR	Surface Plasmon Resonance
SPS/PDAC	Sulfonated Polystyrene/Poly(Diallyl-dimethylammonium Chloride)
St-d35	Stearic Acid-d35
TAZ	Triaminotriazine
TEOA	Triethanolamine
UV–Vis	Ultraviolet–Visible
XPS	X-ray Photoelectron Spectroscopy
YBCO	$YBa_2Cu_3O_7$
ZP	Zirconium Phosphonate
8A5	4-octyl-4′-(5-carboxypentamethyleneoxy)-azobenzene
15,9-DA	Dinonacosa-10,12-diyn-disulfide

REFERENCES

1. A. Ulman 'An Introduction to Ultrathin Organic Films from Langmuir–Blodgett to Self-assembly', Academic Press, San Diego (1991).
2. A. Ulman 'Characterization of Organic Thin Films', Butterworth-Heinemann, Boston (1995).
3. A. Ulman, *Chem. Rev.*, **96**, 1533 (1996).
4. R.A. Dluhy, 'Infrared Spectroscopy of Biophysical Monomolecular Films at Interfaces: Theory and Applications', in "Physical Chemistry of Biological Interfaces", eds A. Baszhin and W. Norde, Marcel Dekker, Inc., New York, 711–747, Chapter 21 (2000).
5. A.G. Frutos, J.M. Brockman and R.M. Corn, *Langmuir*, **16**, 2192 (2000).
6. V.G. Gregoriou, R. Hapanowicz, P.Y. Chen, S.L. Clark and P.T. Hammond, *Annu. Tech. Conf. - Soc. Plast. Eng.*, **2**, 2485 (1999).
7. V.G. Gregoriou, R. Hapanowicz, S.L. Clark and P.T. Hammond, *Appl. Spectrosc.*, **51**, 470 (1997).
8. D.G. Hanken, R.R. Naujok, J.M. Gray and R.M. Corn, *Anal. Chem.*, **69**, 240 (1997).
9. P. Boehme, G. Vedantham, T. Przybycien and G. Belfort, *Langmuir*, **15**, 5323 (1999).
10. T. Morita, S. Kimura, S. Kobayashi and Y. Imanishi, *J. Am. Chem. Soc.*, **122**, 2850 (2000).
11. T. Nakanishi, B. Ohtani and K. Uosaki, *J. Phys. Chem. B*, **102**, 1571 (1998).
12. D.G. Hanken and R.M. Corn, *Anal. Chem.*, **67**, 3767 (1995).
13. H.Z. Yu, H.L. Zhang, Z.F. Liu, S. Ye and K. Uosaki, *Langmuir*, **14**, 619 (1998).
14. Y.S. Shon, S. Lee, S.S. Perry and T.R. Lee, *J. Am. Chem. Soc.*, **122**, 1278 (2000).
15. R. Colorado, Jr, M. Graupe, M. Takenaga, T. Koini and T.R. Lee, 'Surface Dipoles Influence the Wettability of Terminally Fluorinated Organic Films', in "Materials Research Society Symposium Proceedings, 546 (Materials Science of Microelectromechanical Systems (MEMS) Devices)", eds A.H. Heuer and S.J. Jacobs, Materials Research Society, Warrendale, PA, 237–242 (1999).
16. Y.S. Shon, R. Colorado, Jr, C.T. Williams, C.D. Bain and T.R. Lee, *Langmuir*, **16**, 541 (2000).
17. Y.S. Shon and T.R. Lee, *Langmuir*, **15**, 1136 (1999).
18. R. Colorado, Jr, R.J. Villazana and T.R. Lee, *Langmuir*, **14**, 6337 (1998).
19. M.R. Anderson, M.N. Evaniak and M. Zhang, *Langmuir*, **12**, 2327 (1996).
20. N. Garg, J.M. Friedman and T.R. Lee, *Langmuir*, **16**, 4266 (2000).
21. H.L. Zhang, M. Chen and H.L. Li, *J. Phys. Chem. B*, **104**, 28 (2000).
22. Y.S. Shon, N. Garg, R. Colorado, Jr, R.J. Villazana and T.R. Lee, 'Self-assembled Monolayers Derived from Bidentate Organosulfur Adsorbates', in "Materials Research Society Symposium Proceedings, 576 (Organic/Inorganic Hybrid Materials II)", eds L.C. Klein, L.F. Francis and M.R. DeGuire, Materials Research Society, Warrendale, PA, 183–188 (1999).
23. K. Nakano, T. Sato, M. Tazaki and M. Takagi, *Langmuir*, **16**, 2225 (2000).

24. L.J. Fina, J.E. Valentini and Y.S. Tung, 'Structure and Orientation of Surfactant Molecules at the Air–Water Interface', in "Hyphenated Techniques in Polymer Characterization", eds T. Provder, M.W. Urban and H.G. Bath, American Chemical Society, Washington, DC, 44–54 (1994).
25. C.W. Meuse, G. Niaura, M.L. Lewis and A.L. Plant, *Langmuir*, **14**, 1604 (1998).
26. H.L. Zhang, H. Zhang, J. Zhang, H.L. Li and Z.F. Liu, *Mater. Sci. Eng., C*, **C8–C9**, 187 (1999).
27. H.L. Zhang, J. Zhang, H.Y. Li, Z.F. Liu and H.L. Li, *Mater. Sci. Eng., C*, **C8–C9**, 179 (1999).
28. S.W. Han, C.H. Kim, S.H. Hong, Y.K. Chung and K. Kim, *Langmuir*, **15**, 1579 (1999).
29. J. Zhang, H.L. Zhang, M. Chen, J. Zhao, Z.F. Liu and H.L. Li, *Ber. Bunsen-Ges. Phys. Chem.*, **102**, 701 (1998).
30. K. Kobayashi, J. Umemura, T. Horiuchi, H. Yamada and K. Matsushige, *Jpn. J. Appl. Phys., Part 2*, **37**, L297 (1998).
31. J.W.M. Nissink and J.H. Van Der Maas, *Appl. Spectrosc.*, **53**, 33 (1999).
32. M. Kawasaki, T. Sato, T. Tanaka and K. Takao, *Langmuir*, **16**, 1719 (2000).
33. D.J. Revell, I. Chambrier, M.J. Cook and D.A. Russell, *J. Mater. Chem.*, **10**, 31 (2000).
34. A.E. Strong and B.D. Moore, *J. Mater. Chem.*, **9**, 1097 (1999).
35. N. Choi, T. Ishida, A. Inoue, W. Mizutani and H. Tokumoto, *J. Appl. Surf. Sci.*, **144–145**, 445 (1999).
36. J.E. Ritchie, C.A. Wells, D.R. Kanis and J.T. McDevitt, 'Structural Characteristics of Self-assembled Monolayers on a High-Tc Superconductor Probed by Reflection-absorption Infrared Spectroscopy', in "Spectroscopy of Superconducting Materials", ed. E. Faulques, American Chemical Society, Washington, DC, 168–179 (1999).
37. T. Vallant, J. Kattner, H. Brunner, U. Mayer and H. Hoffmann, *Langmuir*, **15**, 5339 (1999).
38. K. Ataka, Y. Hara and M. Osawa, *J. Electroanal. Chem.*, **473**, 34 (1999).
39. H. Skulason and C.D. Frisbie, *Langmuir*, **14**, 5834 (1998).
40. M.R. Anderson and M. Gatin, *Langmuir*, **10**, 1638 (1994).
41. R.C. Sabapathy, S. Bhattacharyya, M.C. Leavy, W.E. Cleland, Jr and C.L. Hussey, *Langmuir*, **14**, 124 (1998).
42. S. Ye, A. Yashiro, Y. Sato and K. Uosaki, *J. Chem. Soc., Faraday Trans.*, **92**, 3813 (1996).
43. K. Bandyopadhyay, L. Shu, H. Liu and L. Echegoyen, *Langmuir*, **16**, 2706 (2000).
44. D.J. Revell, J.R. Knight, D.J. Blyth, A.H. Haines and D.A. Russell, *Langmuir*, **14**, 4517 (1998).
45. R.C. Sabapathy, S. Bhattacharyya, W.E. Cleland, Jr and C.L. Hussey, *Langmuir*, **14**, 3797 (1998).
46. L. Bertilsson, K. Potje-Kamloth, H.D. Liess, I. Engquist and B. Liedberg, *J. Phys. Chem. B*, **102**, 1260 (1998).
47. J.D. Swalen, *Surfactants Solution*, **11**, 41 (1991).
48. T. Takenaka and J. Umemura, *Stud. Interface Sci.*, **4**, 145 (1996).
49. G. Xu, Z. Bao and J.T. Groves, *Langmuir*, **16**, 1834 (2000).
50. T. Hasegawa, D.A. Myrzakozha, T. Imae, J. Nishijo and Y. Ozaki, *J. Phys. Chem. B*, **103**, 11 124 (1999).
51. S. Payan, B. Desbat, C. Destrade and H.T. Nguyen, *Langmuir*, **12**, 6627 (1996).
52. A. Saito, Y. Urai and K. Itoh, *Langmuir*, **12**, 3938 (1996).
53. M. Yamamoto, N. Furuyama and K. Itoh, *J. Phys. Chem.*, **100**, 18 483 (1996).
54. K. Itoh, M. Yamamoto, N. Furuyama and A. Saito, 'Infrared Reflection Absorption Spectroscopic Study on Photochemical Processes in Langmuir–Blodgett Films', in "Progress in Fourier Transform Spectroscopy", eds J. Mink, G. Keresztury and R. Kellner, Springer-Verlag, Vienna, Austria, 33–42 (1997).
55. T. Kawai, *J. Phys. Chem. B*, **103**, 5517 (1999).
56. B. Zhao, H. Li, X. Zhang, J. Shen and Y. Ozaki, *J. Phys. Chem. B*, **102**, 6515 (1998).
57. A. Aoki, N. Moriyama, M. Hironobu and T. Miyashita, *Polym. Prepr. (Am. Chem. Soc., Div. Polym. Chem.)*, **40**, 445 (1999).
58. Y. Guo, F. Feng and T. Miyashita, *Bull. Chem. Soc. Jpn.*, **72**, 2149 (1999).
59. J. Zhai, L.B. Gan and C.H. Huang, *Appl. Surf. Sci.*, **140**, 223 (1999).
60. Y. Wang, K. Nichogi, K. Iriyama and Y. Ozaki, *Mol. Cryst. Liq. Cryst. Sci. Technol., Sect. A*, **294**, 177 (1997).
61. T. Hasegawa, Y. Hatada, J. Nishijo, J. Umemura, Q. Huo and R.M. Leblanc, *J. Phys. Chem. B*, **103**, 7505 (1999).
62. D.A. Myrzakozha, T. Hasegawa, J. Nishijo, T. Imae and Y. Ozaki, *Langmuir*, **15**, 6890 (1999).
63. X. Li, B. Zhao, Y. Wu, W. Xu, G. Li and B. Li, *Spectrosc. Lett.*, **31**, 253 (1998).
64. Z. Zhang, K. Nakashima, A.L. Verma, M. Yoneyama, K. Iriyama and Y. Ozaki, *Langmuir*, **14**, 1177 (1998).
65. S. Ye, Y. Sato and K. Uosaki, *Langmuir*, **13**, 3157 (1997).
66. A. Horn, *Adv. Spectrosc.*, **26**, 273 (1998).
67. R. Mendelsohn, J.W. Brauner and A. Gericke, *Annu. Rev. Phys. Chem.*, **46**, 305 (1995).
68. M.K. Debe, *Prog. Surf. Sci.*, **24**, 1 (1987).
69. J.F. Rabolt, *MRS Bull.*, **12**, 39 (1987).
70. J.D. Swalen, *Springer Ser. Surf. Sci.*, **3**, 248 (1985).
71. B.H. Cumpston and K.F. Jensen, *Synth. Met.*, **73**, 195 (1995).
72. J. Meichsner, *Contrib. Plasma Phys.*, **39**, 427 (1999).
73. A.P. Kam, R. Aroca, J. Duff and C.P. Tripp, *Langmuir*, **16**, 1185 (2000).
74. S. Rodriguez-Llorente, R. Aroca and J. Duff, *Spectrochim. Acta, Part A*, **55A**, 969 (1999).
75. S. Rodriguez-Llorente, R. Aroca and J. Duff, *J. Mater. Chem.*, **8**, 2175 (1998).
76. A. Kam, R. Aroca, J. Duff and C.P. Tripp, *Chem. Mater.*, **10**, 172 (1998).

77. W.N. Richmond, P.W. Faguy and S.C. Weibel, *J. Electroanal. Chem.*, **448**, 237 (1998).
78. I. Cornut, B. Desbat, J.M. Turlet and J. Dufourcq, *Biophys. J.*, **70**, 305 (1996).
79. Y. Yoshida, K. Ishida, K. Ishizaki, T. Horiuchi and K. Matsushige, *Jpn. J. Appl. Phys., Part 1*, **36**, 7389 (1997).
80. P. Allongue, M. Delamar, B. Desbat, O. Fagebaume, R. Hitmi, J. Pinson and J.M. Saveant, *J. Am. Chem. Soc.*, **119**, 201 (1997).
81. Y. Cheng and R.M. Corn, *J. Phys. Chem. B*, **103**, 8726 (1999).
82. D. Blaudez, J.M. Turlet, J. Dufourcq, D. Bard, T. Buffeteau and B. Desbat, *J. Chem. Soc., Faraday Trans.*, **92**, 525 (1996).
83. J. Gallant, B. Desbat, D. Vaknin and C. Salesse, *Biophys. J.*, **75**, 2888 (1998).
84. H. Lavoie, J. Gallant, M. Grandbois, D. Blaudez, B. Desbat, F. Boucher and C. Salesse, *Mater. Sci. Eng., C*, **C10**, 147 (1999).
85. D. Blaudez, F. Boucher, T. Buffeteau, B. Desbat, M. Grandbois and C. Salesse, *Appl. Spectrosc.*, **53**, 1299 (1999).
86. W.-P. Ulrich and H. Vogel, *Biophys. J.*, **76**, 1639 (1999).
87. A. Dicko, H. Bourque and M. Pezolet, *Chem. Phys. Lipids*, **96**, 125 (1998).
88. I. Cornut, B. Desbat, J.M. Turlet and J. Dufourcq, *Biophys. J.*, **70**, 305 (1996).
89. L. Dziri, B. Desbat and R.M. Leblanc, *J. Am. Chem. Soc.*, **121**, 9618 (1999).
90. Y. Xiao, H. Bourque, M. Pezolet and A.M. Ritcey, *Thin Solid Films*, **327–329**, 299 (1998).
91. L. Mao, A.M. Ritcey and B. Desbat, *Langmuir*, **12**, 4754 (1996).
92. C. Alonso, D. Blaudez, B. Desbat, F. Artzner, B. Berge and A. Renault, *Chem. Phys. Lett.*, **284**, 446 (1998).
93. C.Biensan, B. Desbat and J.M. Turlet, *Thin Solid Films*, **284–285**, 293 (1996).
94. Q. Huo, L. Dziri, B. Desbat, K.C. Russell and R.M. Leblanc, *J. Phys. Chem. B*, **103**, 2929 (1999).
95. E. Shirai, Y. Urai and K. Itoh, *J. Phys. Chem. B*, **102**, 3765 (1998).
96. M. Cai, M.D. Mowery, H. Menzel and C.E. Evans, *Langmuir*, **15**, 1215 (1999).
97. M. Cai, M. Ho and J.E. Pemberton, *Langmuir*, **16**, 3446 (2000).
98. M. Cai, M.D. Mowery, J.E. Pemberton and C.E. Evans, *Appl. Spectrosc.*, **54**, 31 (2000).
99. C.E. Taylor, M.H. Schoenfisch and J.E. Pemberton, *Langmuir*, **16**, 2902 (2000).
100. Y. Nagasoe, N. Ichiyanagi, H. Okabayashi, S. Nave, J. Eastoe and C.J. O'Connor, *Phys. Chem. Chem. Phys.*, **1**, 4395 (1999).
101. K. Nishiyama, S.I. Tahara, Y. Uchida, S. Tanoue and I. Taniguchi, *J. Electroanal. Chem.*, **478**, 83 (1999).
102. M. Lewis, M. Tarlov and K. Carron, *J. Am. Chem. Soc.*, **117**, 9574 (1995).
103. M.H. Schoenfisch and J.E. Pemberton, *Langmuir*, **15**, 509 (1999).
104. H. Yamamoto, Y. Maeda and H. Kitano, *J. Phys. Chem. B*, **101**, 6855 (1997).
105. X.M. Yang, D.A. Tryk, K. Hashimoto and A. Fujishima, 'Surface Enhanced Raman Imaging of Patterned Self-assembled Monolayers', in "Microstructures and Microfabricated Systems III", eds P.J. Hesketh, G. Barna and H.G. Hughes, The Electrochemical Society, Pennington, NJ, 159–165 (1997).
106. T. Kim, Q. Ye, L. Sun, K.C. Chan and R.M. Crooks, *Langmuir*, **12**, 6065 (1996).
107. J.F. Ford, T.J. Vickers, C.K. Mann and J.B. Schlenoff, *Langmuir*, **12**, 1944 (1996).
108. X. Tang, T. Schneider and D.A. Buttry, *Langmuir*, **10**, 2235 (1994).
109. N. Sandhyarani and T. Pradeep, *Vacuum*, **49**, 279 (1998).
110. M.H. Schoenfisch and J.E. Pemberton, *J. Am. Chem. Soc.*, **120**, 4502 (1998).
111. C.A. Szafranski, W. Tanner, P.E. Laibinis and R.L. Garrell, *Langmuir*, **14**, 3580 (1998).
112. K. Bandyopadhyay, K. Vijayamohanan, M. Venkataramanan and T. Pradeep, *Langmuir*, **15**, 5314 (1999).
113. F.K. Huang, R.C. Horton, Jr, D.C. Myles and R.L. Garrell, *Langmuir*, **14**, 4802 (1998).
114. J. Chowdhury, P. Pal and T.N. Misra, *Indian J. Phys., B*, **72B**, 615 (1998).
115. H. Jeong, Y.S. Kwon, B.J. Lee and C.S. Ha, *Mol. Cryst. Liq. Cryst. Sci. Technol., Sect. A*, **295**, 443 (1997).
116. J.H. Im, S.H. Park and J.H. Kim, *Mol. Cryst. Liq. Cryst. Sci. Technol., Sect. A*, **294**, 59 (1997).
117. G.G. Siu, Y. Liu, S. Xie, J. Xu, T. Li and L. Xu, *Thin Solid Films*, **274**, 147 (1996).
118. W.W. Zhao and F.J. Boerio, *Surf. Interface Anal.*, **26**, 316 (1998).
119. E. Johnson and R. Aroca, *Langmuir*, **11**, 1693 (1995).
120. R. Aroca, E. Johnson and A.K. Maiti, *Appl. Spectrosc.*, **49**, 466 (1995).
121. C.L. Leverette and R.A. Dluhy, *Langmuir*, **16**, 3977 (2000).
122. O. Stenzel, A. Stendal, D. Drews, T. Werninghaus, M. Falke, D.R.T. Zahn and C. von Borczyskowski, *Appl. Surf. Sci.*, **108**, 71 (1997).
123. J. Chlistunoff, D. Cliffel and A.J. Bard, *Thin Solid Films*, **257**, 166 (1995).
124. S.E.J. Bell, M.D. Devenney, J. Grimshaw, S. Hara, J.H. Rice and J. Trocha-Grimshaw, *J. Chem. Soc., Faraday Trans.*, **94**, 2955 (1998).